AD-A275 152

AD_____

GRANT NO: DAMD17-93-J-3003

TITLE: WAVELET REPRESENTATIONS FOR DIGITAL MAMMOGRAPH

PRINCIPAL INVESTIGATOR: Andrew F. Laine

CONTRACTING ORGANIZATION: University of Florida
219 Grinter Hall
Gainesville, Florida 32611

REPORT DATE: December 15, 1993

TYPE OF REPORT: Annual Report

DTIC SELECTE
JAN 3 1 1994
B
D

PREPARED FOR: U.S. Army Medical Research and
Development Command, Fort Detrick
Frederick, Maryland 21702-5012

DISTRIBUTION STATEMENT: Approved for public release;
distribution unlimited

The views, opinions and/or findings contained in this report are
those of the author(s) and should not be construed as an official
Department of the Army position, policy or decision unless so
designated by other documentation.

i

40pg **94-02748**

94 1 27 002

REPORT DOCUMENTATION PAGE

Public reporting burden for this collection of information is estimated to average 1 hour per response, including the time for reviewing instructions, searching existing data sources, gathering and maintaining the data needed, and completing and reviewing the collection of information. Send comments regarding this burden estimate or any other aspect of this collection of information, including suggestions for reducing this burden to Washington Headquarters Services, Directorate for Information Operations and Reports, 1215 Jefferson Davis Highway, Suite 1204, Arlington, VA 22202-4302, and to the Office of Management and Budget, Paperwork Reduction Project (0704-0188), Washington, DC 20503.

1. AGENCY USE ONLY (Leave blank)	2. REPORT DATE	3. REPORT TYPE AND DATES COVERED
	15 December 1993	Annual (11/16/92 – 11/15/93)

4. TITLE AND SUBTITLE
Wavelet Representations for Digital Mammograph

5. FUNDING NUMBERS
Grant No.
DAMD17-93-J-3003

6. AUTHOR(S)
Dr. Andrew F. Laine

7. PERFORMING ORGANIZATION NAME(S) AND ADDRESS(ES)
University of Florida
219 Grinter Hall
Gainesville, Florida 32611

8. PERFORMING ORGANIZATION REPORT NUMBER

9. SPONSORING/MONITORING AGENCY NAME(S) AND ADDRESS(ES)
U.S. Army Medical Research & Development Command
Fort Detrick
Frederick, Maryland 21702-5012

10. SPONSORING/MONITORING AGENCY REPORT NUMBER

11. SUPPLEMENTARY NOTES
Prepared in cooperation with Walter Huda, Ph.D., Janice Honeyman, Ph.D, and Barbara Steinbach, M.D

12a. DISTRIBUTION/AVAILABILITY STATEMENT
Approved for public release; distribution unlimited

12b. DISTRIBUTION CODE

13. ABSTRACT (Maximum 200 words)

This report describes a novel approach for accomplishing mammographic feature analysis by overcomplete multiresolution representations. We show that efficient representations may be identified within a continuum of scale-space and used to enhance features of importance to mammography. We present methods of contrast enhancement based on three overcomplete multiscale representations: (1) the dyadic wavelet transform, (2) the phi-transform, and (3) hexagonal wavelets.

Digital mammograms are reconstructed from wavelet coefficients modified at one or more levels by local and global non-linear operators (multiscale edges and histogram modification). In each case, multiscale edges and gain parameters are identified adaptively by a measure of energy within each level of scale-space. We show quantitatively that transform coefficients, modified within each level by adaptive non-linear operators, can make more obvious unseen or barely seen features of mammography without requiring additional radiation. Our results are compared with traditional image enhancement techniques by measuring the local contrast of known mammographic features. We demonstrate that features extracted from multiresolution representations can provide an adaptive mechanism for accomplishing local contrast enhancement. By improving the visualization of breast pathology we can improve chances of early detection while requiring less time to evaluate mammograms for most patients.

14. SUBJECT TERMS
Wavelet Analysis, Mammography, Contrast enhancement, Multiscale representations, Digital image processing, Breast Cancer, Lab Animals, Mice, RAD VI

15. NUMBER OF PAGES

16. PRICE CODE

17. SECURITY CLASSIFICATION OF REPORT	18. SECURITY CLASSIFICATION OF THIS PAGE	19. SECURITY CLASSIFICATION OF ABSTRACT	20. LIMITATION OF ABSTRACT
Unclassified	Unclassified	Unclassified	Unlimited

NSN 7540-01-280-5500

FOREWORD

Opinions, interpretations, conclusions and recommendations are those of the author and are not necessarily endorsed by the US Army.

___✓___ Where copyrighted material is quoted, permission has been obtained to use such material.

___✓___ Where material from documents designated for limited distribution is quoted, permission has been obtained to use the material.

___✓___ Citations of commercial organizations and trade names in this report do not constitute an official Department of Army endorsement or approval of the products or services of these organizations.

___—___ In conducting research using animals, the investigator(s) adhered to the "Guide for the Care and Use of Laboratory Animals," prepared by the Committee on Care and Use of Laboratory Animals of the Institute of Laboratory Resources, National Research Council (NIH Publication No. 86-23, Revised 1985).

___—___ For the protection of human subjects, the investigator(s) adhered to policies of applicable Federal Law 45 CFR 46.

___—___ In conducting research utilizing recombinant DNA technology, the investigator(s) adhered to current guidelines promulgated by the National Institutes of Health.

___—___ In the conduct of research utilizing recombinant DNA, the investigator(s) adhered to the NIH Guidelines for Research Involving Recombinant DNA Molecules.

___—___ In the conduct of research involving hazardous organisms, the investigator(s) adhered to the CDC-NIH Guide for Biosafety in Microbiological and Biomedical Laboratories.

Accession For	
NTIS GRA&I	☑
DTIC TAB	☐
Unannounced	☐
Justification	
By	
Distribution/	
Availability Codes	
Dist	Avail and/or Special
A-1	

PI - Signature   12/13/93   Date

i

TABLE OF CONTENTS

1 Introduction

Many cancers escape detection due to the density of surrounding breast tissue. For example, differences in attenuation of the various soft tissue structures in the female breast are small, and it is necessary to use low levels of X-ray energy to obtain high contrast in mammographic film. Since contrast between the soft tissues of the breast is inherently low and because relatively minor changes in mammary structure can signify the presence of a malignant breast tumor, the detection is more difficult in mammography than in most other forms of radiography. The radiologist must search for malignancy in mammographic features such as microcalcifications, dominate and stellate masses, as well as textures of fibrous tissues (fibroglandular patterns).

A primary breast carcinoma can metastasize when it consists of a relatively small number of cells, far below our present threshold of detection. The importance of diagnosis of breast cancer at an early stage is critical to patient survival. Despite advances and improvements in mammography and mammographic screening programs, the detection of minimal breast cancer (those cancers 1.0 cm or less in diameter) remains difficult. At present, mammography is capable of detecting some cases through indirect signs, particularly through the presence of characteristic microcalcifications. It has been suggested that as normally viewed, mammograms display only about 3% of the information they detect! [2]. The inability to detect these small tumors motivates the multiscale imaging techniques presented in this report.

Digital image processing techniques have been applied previously to mammography. The focus of past investigations has been to enhance mammographic features while reducing the enhancement of noise. Gordon and Rangayyan [10] used adaptive neighborhood image processing to enhance the contrast of features relevant to mammography. This method enhanced the contrast of mammographic features as well as noise and digitization effects. Dhawan [7, 8, 9] has made significant contributions towards solving problems encountered in mammographic image enhancement. He developed an adaptive neighborhood-based image processing technique that utilized low-level analysis and knowledge about a desired feature in the design of a contrast enhancement function to improve the contrast of specific features. Recently, Tahoces [25] developed a method for the enhancement of chest and breast radiographs by automatic spatial filtering. In their method, they used a linear combination of an original image and two smoothed images obtained from the original image by applying different spatial masks. The process was completed by nonlinear contrast stretching. This spatial filtering enhanced edges while minimally amplifying noise.

Methods of feature enhancement have been key to the success of classification algorithms. Lai [11] compared several image enhancement methods for detecting circumscribed masses in mammograms. They compared an edge-preserving smoothing function [22], a half-neighborhood

method [23], k-nearest neighborhood, directional smoothing [6] and median filtering [3], and in addition proposed a method of selective median filtering.

In the fields of image processing and computer vision, transforms such as the windowed Fourier transforms that can decompose a signal into a set of frequency intervals of constant size have been used in many applications, including image compression and texture analysis. Because the spatial and frequency resolutions of these transforms are constant, the information provided by such decompositions is not localized in the spatial domain. A wavelet transform [4, 5, 17, 18, 19, 20] is a decomposition of an image onto a family of functions called a *wavelet family*. In comparison to a windowed Fourier transform which has a fixed resolution in the spatial and frequency domain, the resolution of a wavelet transform varies with a scale parameter, decomposing an image into a set of frequency channels of constant bandwidth on a logarithmic scale. This variation of resolution enables the wavelet transform to "zoom" into the irregularities of an image and characterize them locally.

In this report we introduce a novel method for accomplishing adaptive contrast enhancement [13, 14, 15]. We describe methods of image enhancement that use separable and non-separable analyzing functions to compute multiscale representations. Mammograms are then reconstructed from transform coefficients modified at each level by both local and global non-linear operators. We show preliminary results that suggest such methods can emphasize significant features in digital mammography for improved visualization of breast pathology.

1.1 Framework for Multiscale Analysis

During the past year we have accomplished mammographic feature analysis through three multiresolution representations: the dyadic wavelet transform, the φ-transform or Frazier-Jawerth transform (FJT) and the hexagonal wavelet transform. By using multiresolution representations, we may decompose an image into a multiresolution hierarchy of localized information at different spatial frequencies. The representations used in our study are more attractive than traditional multiresolution techniques because perfect reconstruction is possible. Our approach for mammographic feature analysis consists of the application of non-linear techniques for image enhancement within levels of a redundant multiresolution representation (frames).

Multiscale wavelet representations suggest a mathematically coherent basis not only for existing multi-grid techniques, but also for exploiting non-linear systems. Multiresolution wavelet analysis provides a natural hierarchy in which to embed an interactive paradigm for accomplishing scale-space feature analysis. Similar to traditional coarse to fine matching strategies, the radiologist may first choose to look for coarse features (e.g. dominant masses) within low frequency levels of the wavelet transform and later examine finer features (e.g. microcalcifications) at higher frequency levels. Choosing wavelets (or analyzing functions) that are simultaneously

localized in both space and frequency, results in a powerful methodology for image analysis. The inner-product of a signal f with a wavelet ψ $\left(\langle f, \psi \rangle = (2\pi)^{-1} \langle \hat{f}, \hat{\psi} \rangle \right)$ reflects the character of f within the time-frequency region where ψ is localized ($\hat{\psi}$ and $\hat{f}$ are the Fourier transforms of the analyzing function and the signal, respectively). If ψ is spatially localized, then two-dimensional features such as shape and orientation are preserved in the transform space and may characterize a feature through scale-space. We may "extract" such features by applying geometric constraints within each level of the transform. We can reduce the complexity of a reconstructed mammogram by selecting only a subset of features that satisfy certain geometric constraints. We may choose to focus on only those features oriented in a particular direction. Subsequent image reconstructions may use the context provided by previously enhanced features to examine (diagnose) additional features emergent at other scales and orientations. For example, fine vertical features may be selected and analyzed in the context of previously classified large horizontal features. Thus, our strategy provides a global context upon which subtle features within finer scales may be classified incrementally through a precomputed hierarchy of scale-space.

Our approach to feature analysis and classification is motivated in part by recently discovered biological mechanisms of the human visual system [26]. Both multiorientation and multiresolution are known features of the human visual system. There exist cortical neurons which respond specifically to stimuli within certain orientations and frequencies. In this report we exploit the orientation and frequency selectivity of wavelet transforms to make mammographic features more obvious through localized contrast gain.

Below, we present a concise overview of the multiresolution representations used in our study, and introduce the notation used to describe the techniques discussed in later sections. In the next section we address the use of non-linear techniques for image enhancement within the context of multiresolution representations.

A multiresolution representation divides the frequency spectrum of an image x into a low-pass sub-band image y_0^L and a set of band-pass sub-band images y_j^i, $i = 1, \ldots, L$, $j = 1, \ldots, M$, where L and M denote the number of levels and orientations for a representation, respectively. Notice that a sub-band image without orientation selectivity is denoted by $j = 0$. For example, in the case of an isotropic multiresolution decomposition, $j = 0$ for all levels of the representation. In general, multiresolution representations are implemented by a cascade of analysis/synthesis (A/S) filter banks. For example, Figure 1 shows the implementation of a two-level ($L = 2$) multiresolution representation which partitions orientations into three bands ($M = 3$) by using a cascade of two 4-channel A/S filter banks. The analysis filters, denoted by F, are used to compute the multiresolution decomposition of an image x, while the synthesis filters, denoted by G, are used to reconstruct the original image from its multiresolution representation (transform coefficients). Both, analysis and synthesis sections of the A/S filter bank form a band-splitting
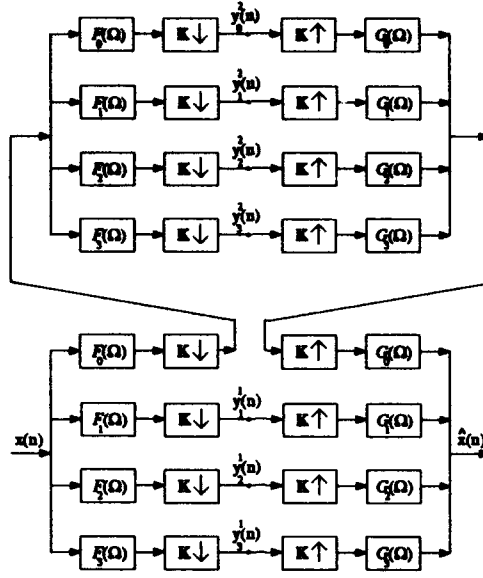
3

Figure 1: A two-level 4-channel analysis/synthesis filter bank.

system consisting of one low-pass filter, denoted by F_0 and G_0, respectively, and M band-pass filters, denoted by F_i and G_i, $i = 1, \ldots, M$, respectively. Notice that the A/S filter banks are cascaded hierarchically through the low-pass band of the filter bank in order to accomplish a multiresolution representation.

Let F_j^i and G_j^i denote the equivalent filters for the ith level and j^{th} channel of a cascade of analysis and synthesis filters, respectively. Let $W_{ij}[x]$ denote the operation of filtering x with the equivalent filter F_j^i. Then, the sub-band images of an L-level multiresolution decomposition are given by

$$y_j^i = W_{ij}[x].$$ (1)

Similarly, let $W_{ij}^{-1}[y]$ denote the operation of filtering image y with the equivalent filter G_j^i. Then, an L-level multiresolution reconstruction may be written as

$$x = W_{L0}^{-1}[y_0^L] + \sum_{i=1}^{L} \sum_{j=1}^{M} W_{ij}^{-1}[y_j^i].$$ (2)

By combining equations (1) and (2) we obtain the general expression for an L-level multiresolution decomposition and reconstruction

$$x = W_{L0}^{-1}[W_{L0}[x]] + \sum_{i=1}^{L} \sum_{j=1}^{M} W_{ij}^{-1}[W_{ij}[x]].$$ (3)

The three multiscale transforms used in our study shall follow the general formulation presented above, but are characterized by distinct analysis/synthesis filter banks. In the following subsections, we provide a brief overview of the mathematical formulation for each of the filter

4

banks used in our investigation. For consistency and clarity, we adopt the above notation throughout the report.

1.1.1 Dyadic Wavelet Transform

In [16], Mallat showed that a two-dimensional dyadic wavelet transform can be easily constructed from one-dimensional wavelets. Suppose A and B are one-dimensional low-pass and high-pass filters, respectively. Furthermore, suppose that A and B satisfy $|A(\omega)|^2 + |B(\omega)|^2 = 1$. Then, two-dimensional analysis filters implementing a dyadic wavelet transform may be given by

$$F_0(\omega_x, \omega_y) = A(\omega_x) \otimes A(\omega_y), \ F_1(\omega_x, \omega_y) = B(\omega_x) \otimes C(\omega_y), \text{ and } F_2(\omega_x, \omega_y) = C(\omega_x) \otimes B(\omega_y),$$

where $Q \otimes R$ denotes the tensor product of Q and R, and $C(\omega)$ is the transfer function of a one-dimensional discrete filter satisfying

$$|C(\omega)|^2 = \frac{1 + |A(\omega)|^2}{2}.$$

Synthesis filters are easily obtained by

$$G_i(\omega_x, \omega_y) = \overline{F_i(\omega_x, \omega_y)}, \ i = 0, 1, 2,$$

where $\overline{Q}$ denotes the complex conjugate of Q.

Hence, a two-dimensional dyadic wavelet transform results in a multiresolution representation which partitions orientations into two bands ($M = 2$). Figure 2 displays the magnitude of the equivalent filters F_j^i for levels 1, 2, and 3, and clearly shows that for the dyadic wavelet transform, orientations are partitioned into horizontal and vertical bands.

In the next subsubsections we describe two non-separable multiscale representations useful for improving local contrast in digital mammography.

1.1.2 φ-Transform

In [12], Laine showed that a two-dimensional φ-transform may be implemented by an analysis/synthesis filter bank constructed from isotropic filters ($M = 0$). In this case, the general expression for an L-level multiresolution decomposition and reconstruction is simply reduced to

$$x = \sum_{i=1}^{L} W_i^{-1} \left[W_i[x] \right],$$

where the subindex j has been suppressed for clarity.

A useful set of equivalent analysis filters for an L-level φ-transform is given by

$$F^i(\omega_x, \omega_y) = \begin{cases} \sqrt{\frac{1}{2} \left[1 - cos \left(\pi \log_2 \left(\frac{2^{i-2} \sqrt{|\omega_x|^2 + |\omega_y|^2}}{\pi} \right) \right) \right]}, & \text{for } \frac{\pi}{2^i} \leq \sqrt{|\omega_x|^2 + |\omega_y|^2} \leq \frac{\pi}{2^{i-2}}, \\ 0, & \text{otherwise,} \end{cases}$$
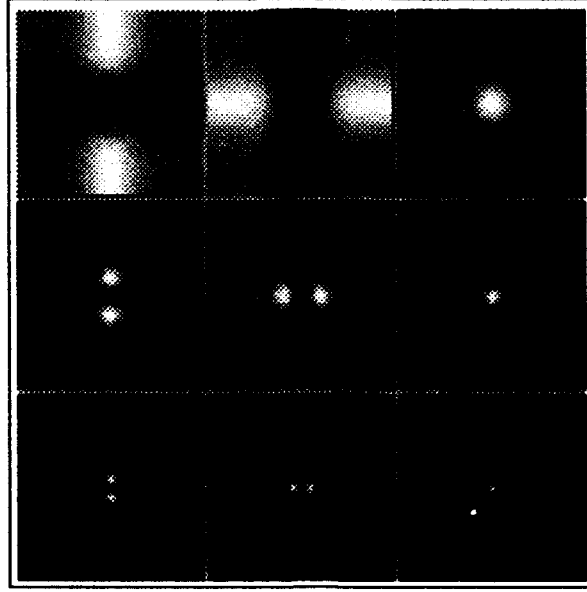
5

Figure 2: Analyzing filters F_j^i used in the dyadic wavelet transform. From top to bottom, $i = 1$, $i = 2$ and $i = 3$. From left to right $j = 2$, $j = 1$ and $j = 0$.
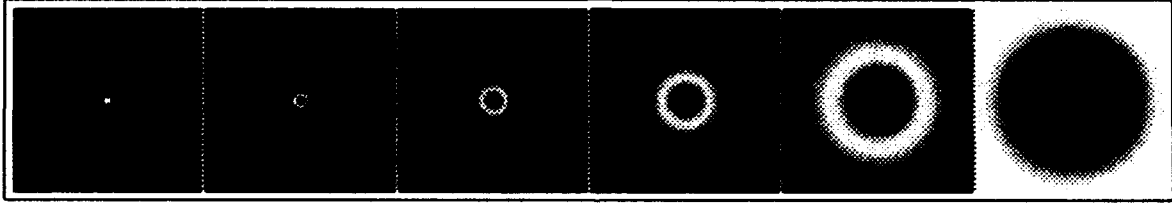

Figure 3: Analyzing filters F^i used in the φ-transform. From left to right, F^6 through F^1.

for $2 \leq i \leq L - 1$. For $i = 1$ and $i = L$ we have

$$F^1(\omega_x, \omega_y) = \begin{cases} \sqrt{1 - (F^2(\omega_x, \omega_y))^2}, & \text{for } \frac{\pi}{2} \leq \sqrt{|\omega_x|^2 + |\omega_y|^2}, \ |\omega_x| \leq \pi, \ |\omega_y| \leq \pi \\ 0, & \text{otherwise,} \end{cases}$$

and

$$F^L(\omega_x, \omega_y) = \begin{cases} \sqrt{1 - (F^{L-1}(\omega_x, \omega_y))^2}, & \text{for } 0 \leq \sqrt{|\omega_x|^2 + |\omega_y|^2} \leq \frac{\pi}{2^{L-2}}, \\ 0, & \text{otherwise,} \end{cases}$$

respectively. Equivalent synthesis filters are easily obtained by computing

$$G^i(\omega_x, \omega_y) = F^i(\omega_x, \omega_y), \quad i = 1, \ldots, L.$$

Figure 3 shows the magnitude of the equivalent filters F^i for levels 1 through 6.

1.1.3 Hexagonal Wavelet Transform

In [1], Adelson showed that it is possible to develop non-separable multiresolution representations based on hexagonally symmetric analysis/synthesis filter banks. Simoncelli [24] showed that a
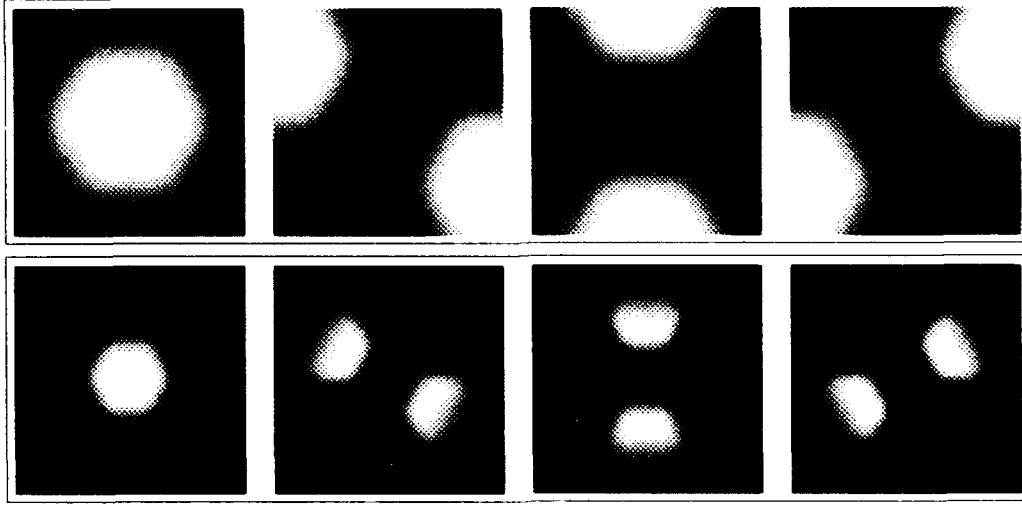
Figure 4: Analyzing filters F_j^i used in the hexagonal wavelet transform. From top to bottom, $i = 1$ and $i = 2$. From left to right $j = 0$, $j = 1$, $j = 2$ and $j = 3$.

solution to the hexagonal analysis/synthesis filter bank is given by

$$
\begin{aligned}
F_0(\mathbf{\Omega}) &= G_0(-\mathbf{\Omega}) &&= H(\mathbf{\Omega}) = H(-\mathbf{\Omega}) \\
F_1(\mathbf{\Omega}) &= G_1(-\mathbf{\Omega}) &&= \exp(-j\mathbf{\Omega}^{\mathrm{T}}\mathbf{s}_1)H(\mathbf{\Omega} - \mathbf{k}_1^h) \\
F_2(\mathbf{\Omega}) &= G_2(-\mathbf{\Omega}) &&= \exp(-j\mathbf{\Omega}^{\mathrm{T}}\mathbf{s}_2)H(\mathbf{\Omega} - \mathbf{k}_2^h) \\
F_3(\mathbf{\Omega}) &= G_3(-\mathbf{\Omega}) &&= \exp(-j\mathbf{\Omega}^{\mathrm{T}}\mathbf{s}_3)H(\mathbf{\Omega} - \mathbf{k}_3^h),
\end{aligned}
$$

where $\mathbf{\Omega} = [\omega_x \ \omega_y]^{\mathrm{T}}$ and

$$
\mathbf{s}_1 = \begin{bmatrix} 1 \\ 0 \end{bmatrix}, \quad \mathbf{s}_2 = \begin{bmatrix} \frac{1}{2} \\ \frac{\sqrt{3}}{2} \end{bmatrix}, \text{ and } \mathbf{s}_3 = \begin{bmatrix} \frac{1}{2} \\ -\frac{\sqrt{3}}{2} \end{bmatrix},
$$

for

$$
\mathbf{k}_1^h = \begin{bmatrix} \pi \\ \frac{\pi}{\sqrt{3}} \end{bmatrix}, \quad \mathbf{k}_2^h = \begin{bmatrix} 0 \\ \frac{2\pi}{\sqrt{3}} \end{bmatrix}, \text{ and } \mathbf{k}_3^h = \begin{bmatrix} \pi \\ \frac{3\pi}{\sqrt{3}} \end{bmatrix}.
$$

A low-pass solution for $H(\mathbf{\Omega})$ in the above equations results in a band-splitting system which may be cascaded hierarchically through the low-pass band of the A/S filter bank to produce a multiresolution representation which partitions orientations into three bands ($M = 3$) of 60 degrees. In our study we used hexagonal A/S filter banks with small regions of support for which perfect reconstruction was well approximated [24]. Figure 4 shows the magnitude of the equivalent hexagonal filters F^i for levels 1 and 2.

In the next section, we describe techniques for modifying transform coefficients within *wavelet frames* for contrast enhancement. The first method allows us to emphasize the structure of local features (singularities) within distinct level of scale-space while the second method is more global in nature.

2 Body

In this section we describe a general method to accomplish multiscale contrast enhancement. Here, non-linear techniques for image enhancement are applied within the context of multiresolution representations. Below we present a general formula for processing sub-band images to accomplish adaptive contrast enhancement of digital mammography. Let f be a user defined function designed to emphasize features of importance within a selected level i. Then, enhanced sub-band images $\hat{y}_j^i$ may be given by

$$\hat{y}_j^i = f(y_j^i). \tag{4}$$

Thus, we obtain an enhanced image $\hat{x}$ from its multiresolution representation by replacing in equation (2) selected sub-band images y_j^i with their enhanced counterparts $\hat{y}_j^i$. In particular, the image enhancement techniques described below are applied only to band-pass sub-band images of a multiresolution representation. In general, by defining the function f, we can denote specific enhancement schemes for modifying sub-band image coefficients within distinct levels of scale-space.

2.1 Local Enhancement Techniques

A problem for image enhancement in digital mammography is the ability to emphasize mammographic features while *reducing* the enhancement of noise. Multiscale representations localize mammographic features. Previously [14, 15], we presented a local enhancement technique for digital mammography based on multiscale edges. In this study, enhanced sub-band images $\hat{y}_j^i = f(y_j^i)$ were given by

$$\hat{y}_j^i(n_1, n_2) = \begin{cases} y_j^i(n_1, n_2), & \text{if } e_j^i(n_1, n_2) \le T_j^i, \\ g_j^i \, y_j^i(n_1, n_2), & \text{if } e_j^i(n_1, n_2) > T_j^i, \end{cases}$$

where e_j^i is the the edge set corresponding to y_j^i, and g_i and T_j^i are the local gain and threshold at level i, respectively. Formal definitions of the edge set for each of the multiscale representations used in this investigation are presented in the next subsections. Multiscale edges e_j^i are used as an "index" to increase the local gain of sub-band image coefficients and to emphasize significant features "living" within level i of the transform space. We have found that an effective strategy to adaptively select the threshold value is to set T_j^i proportional to the standard deviation of pixel values in each y_j^i, that is

$$T_j^i = \frac{1}{2} \sqrt{ \frac{1}{N^2} \sum_{n_1=1}^{N} \sum_{n_2=1}^{N} \left(y_j^i(n_1, n_2) - m_y \right)^2 }$$

where m_y is the mean value of y_j^i and $N \times N$ is the size of the image. Thus for each band-pass image the threshold value is directly related to the energy of the image within that band (wavelet

sub-space). Similarly, g_j^i may be bound adaptively by

$$g_j^i = \frac{T_j^{i\,max}}{T_j^i},$$

where

$$T_j^{i\,max} = \max\{T_j^i, 1 \le i \le L\}$$

for $j = 1, \ldots, M$.

In the next section, we describe how e_j^i was obtained for each of the multiscale representations used in our investigation.

2.1.1 Dyadic Wavelet Multiscale Edges

For the dyadic wavelet transform [16] we compute multiscale edges by detecting the modulus μ^i and angle α^i of sub-band images y_1^i and y_2^i as follows

$$\mu^i(n_1, n_2) = \sqrt{(y_1^i(n_1, n_2))^2 + (y_2^i(n_1, n_2))^2}$$

$$\alpha^i(n_1, n_2) = \arctan\left(\frac{y_2^i(n_1, n_2)}{y_1^i(n_1, n_2)}\right),$$

where $\alpha^i(n_1, n_2)$ is approximated to the closest orientation defined over an eight pixel neighborhood. At level i we define the dyadic-maxima $m^i(n_1, n_2)$ as

$$m^i(n_1, n_2) = \begin{cases} \mu^i(n_1, n_2), & \text{if } \mu^i(n_1, n_2) \text{ is maximum along the} \\ & \text{gradient direction } \alpha^i(n_1, n_2), \\ 0, & \text{otherwise.} \end{cases}$$

Multiscale edges at level i were then obtained by $e_1^i = e_2^i = m^i$. Figure 6 shows the set of images used to identify two-dimensional wavelet-maxima coefficients for the mammogram shown in Figure 9. The photographs shown in the leftmost column were obtained by combining wavelet coefficients oriented along the x and y directions. Thus, a single picture is shown for each distinct level. Note the clear geometric shape of the calcifications seen at the finer levels of the scale-space and the definition of the fibroglandular patterns throughout the dense tissue. The photographs in the middle column show the orientation of the coefficients at each level. For purpose of display, the range 0 to 360 degrees has been mapped onto the gray scale values 0 to 255. The wavelet-maxima coefficients are shown as binary images in the rightmost column of Figure 6. As mentioned earlier, these representations shall define a local index for an adaptive weight function applied to corresponding wavelet coefficients within each level of a transform space.

2.1.2 φ-Transform Multiscale Edges

For the φ-transform we compute multiscale edges e^i by first detecting the φ-maxima along four distinct directions defined as follows

$$m_1^i(n_1, n_2) = \begin{cases} |y^i(n_1, n_2)|, & \text{if } |y^i(n_1, n_2)| > |y^i(n_1 + 1, n_2)| \text{ and} \\ & |y^i(n_1, n_2)| > |y^i(n_1 - 1, n_2)|, \\ 0, & \text{otherwise,} \end{cases}$$

$$m_2^i(n_1, n_2) = \begin{cases} |y^i(n_1, n_2)|, & \text{if } |y^i(n_1, n_2)| > |y^i(n_1 + 1, n_2 + 1)| \text{ and} \\ & |y^i(n_1, n_2)| > |y^i(n_1 - 1, n_2 - 1)|, \\ 0, & \text{otherwise,} \end{cases}$$

$$m_3^i(n_1, n_2) = \begin{cases} |y^i(n_1, n_2)|, & \text{if } |y^i(n_1, n_2)| > |y^i(n_1, n_2 + 1)| \text{ and} \\ & |y^i(n_1, n_2)| > |y^i(n_1, n_2 - 1)|, \\ 0, & \text{otherwise,} \end{cases}$$

$$m_4^i(n_1, n_2) = \begin{cases} |y^i(n_1, n_2)|, & \text{if } |y^i(n_1, n_2)| > |y^i(n_1 + 1, n_2 - 1)| \text{ and} \\ & |y^i(n_1, n_2)| > |y^i(n_1 - 1, n_2 + 1)|, \\ 0, & \text{otherwise.} \end{cases}$$

Multiscale edges at level i are then obtained by combining the φ-maxima of distinct orientations at each level of the transform by

$$e^i = m_1^i + m_2^i + m_3^i + m_4^i.$$

Figure 7 shows the combined φ-maxima edges (adaptively thresholded) at level 4 for the mammogram shown in Figure 10.

2.1.3 Hexagonal Wavelet Multiscale Edges

For the hexagonal wavelet transform, sub-band images y_1^i, y_2^i and y_3^i partition orientations into 60, 0 and -60 degree bands, respectively. Multiscale edges e_1^i, e_2^i and e_3^i at level i are obtained simply by computing the hexagonal-maxima at 60, 0 and -60 degrees, respectively. Figure 8 shows the union of multiscale edges e_1^i, e_2^i and e_3^i at level 3 for the mammogram shown in Figure 12.

2.2 Global Enhancement Techniques

In this section we present two global enhancement techniques designed in our investigation: multiscale histogram equalization (MHE) and multiscale adaptive gain (MAG).

2.2.1 Multiscale Histogram Equalization

Histogram equalization of sub-band images provides a global method to accomplish multiresolution enhancement. We simply define a cummulative density function f as

$$f(y) = \int_{y_{min}}^{y} \rho_y(w)dw + y_{min},$$

where $\rho_y(w) = p_y(w)(y_{max} - y_{min})$, and $p_y(w)$ is the probability density function of y. Notice that $f(y)$ is a single-valued, monotonically increasing function in the range $[y_{min}, y_{max}]$ and satisfies $f(y_{min}) = y_{min}$, $f(y_{max}) = y_{max}$.

10

2.2.2 Multiscale Adaptive Gain

Histogram equalization enhances all pixels uniformly. In another approach, we suppress pixel values of very small amplitude, and enhance only those pixels that are larger than a certain threshold T within each level of the transform space. Thus, we have designed the following function to accomplish this non-linear operation:

$$f(y) = a \left[\text{sigm}(c(y - b)) - \text{sigm}(-c(y + b)) \right], \tag{5}$$

where

$$a = \frac{1}{\text{sigm}(c(1 - b)) - \text{sigm}(-c(1 + b))},$$
$$0 < b < 1,$$

and $\text{sigm}(y)$ is defined by

$$\text{sigm}(y) = \frac{1}{1 + e^{-y}}.$$

It can be easily shown that $f(y)$ is *continuous* and monotonically increasing within the interval $[-1, 1]$ (similar to histogram equalization). Furthermore, any order derivative of $f(y)$ exists and is continuous. Therefore, enhancement using $f(y)$ will not introduce any new discontinuities. In addition, $f(y)$ satisfies the conditions $f(0) = 0$ and $f(1) = 1$. Figure 5 shows a plot of $f(y)$ for typical values of b and c obtained in our study. Clearly, there always exists a T such that pixel values larger than T are enhanced, while pixel values smaller than T are suppressed. The exact value of T can be obtained by solving the non-linear equation $f(y) - y = 0$. However, for simplicity the threshold is controlled through the parameter b. Similarly, we use the standard deviation of pixel values to adaptively (automatically) select T. Moreover, we define an enhancement rate for $f(y)$ as follows

$$
\begin{aligned}
\left. \frac{df}{dy} \right|_{y=b} &= ac \left[0.25 + \frac{e^{2bc}}{[1 + e^{2bc}]^2} \right] \\
&\approx 0.25\, ac \text{ for } bc > 2.
\end{aligned}
$$

Hence, effective contrast enhancement can be controlled through parameter c alone.

For an input image y with maximum absolute amplitude y_{max}, we map the image range $[-y_{max}, y_{max}]$ onto the interval $[-1, 1]$. This is accomplished by using y_{max} as a normalizing factor in equation (5). Thus, $f(y)$ may be written as

$$f(y) = a\, y_{max} \left[\text{sigm}(c(y/y_{max} - b)) - \text{sigm}(-c(y/y_{max} + b)) \right].$$

The benefit of the normalization is that a, b, and c can be *set independently* of the dynamic range of the input image (a digital radiograph of unknown density).
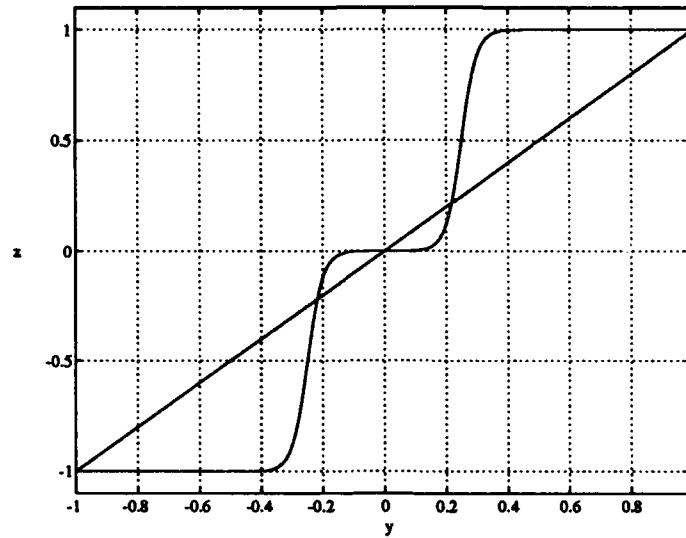
Figure 5: Adaptive gain: $f(y)$ for $b = 0.25$ and $c = 40$ overlayed with $z = y$.

2.3 Experimental Results and Discussion

Preliminary results have shown that the multiscale processing techniques described above, can make more obvious unseen or barely seen features of a mammogram without requiring additional radiation. Our study suggests that the analyzing functions presented in this report can improve the visualization of features of importance to mammography and assist the radiologist in the early detection of breast cancer. In our study, film radiographs of the breast were digitized at 100 micron spot size, on a Kodak laser film digitizer, with 10-bit quantization (contrast resolution). Each digital image was cropped to a matrix size of 512 × 512 before processing.

Figure 9(a) shows a typical radiograph of the breast (poor contrast). Figure 9(c) shows an enhancement obtained from localization defined by two-dimensional multiscale edges of a dyadic transform, shown in Figure 6(c). In this case, wavelet coefficients associated with the multiscale edges from level two alone were modified locally by adaptive scale-space weights, as described in Section 3.1.1. Note that the emphasis on details at level two alone, improved the local contrast of both micro and macro calcification clusters not visible in the original low contrast mammogram. For comparison, Figure 9(b) shows the result of enhancement by unsharp masking. Fewer details are revealed in comparison to the wavelet based method.

Figure 10(a) shows a "dense" mammogram. This class of mammogram is more typical in younger females due to the greater absorption of X-ray energy by less fatty tissues in the breast. They remain particularly difficult to diagnose due to lack of contrast, even for radiologist specializing in mammography. Figure 10(c) shows the result of global wavelet processing for four

12

levels of analysis. In this case, the values of transform coefficients within each level of a dyadic decomposition (excluding the DC cap) were modified by histogram equalization independently. Since the coefficients are space-frequency representations, contrast modifications on the transform side are preserved in part on the spatial side. Similar contrast gains were observed for additional dense radiographs. Figure 10(b) displays the result of standard histogram equalization. Unfortunately, the dense tissues of the breast image are "washed out".

Figure 11(a) shows a mammogram containing a spicular mass. The lack of sharpness is most probably due to poor screen-film contact. Figure 11(c) shows the result of adaptive multiscale processing using the non-separable, non-orthogonal analyzing function described earlier in Section 2.2. In this example, histogram modification was accomplished for an eight level decomposition via the method of multiscale adaptive gain. Radiologist have observed that the subtle features including calcifications and the penetration of fibroglandular structures into the obvious mass tissue are made more clear. In addition, the geometric shape of calcifications (important for diagnosis) are made more visible and improved definition is seen in the ductules (intra and extra lobular units) as well as in the arterial structures within the less dense tissue of the breast. Figure 11(b) shows the result of adaptive histogram equalization. Unfortunately, large areas of the breast are obscured.

Mathematical models of phantoms were constructed to validate our enhancement techniques against false positives arising from possible artifacts introduced by the analyzing functions and to compare our methods against traditional image processing techniques of improving contrast. Our models included features of regular and irregular shapes and sizes of interest in mammographic imaging, such as microcalcifications, cylindrical and spicular objects and conventional masses. Techniques for "blending" a normal mammogram with the images of mathematical models, were developed. The purpose of these experiments was to test the *performance* of our processing techniques on inputs known "a priori" using mammograms where the objects of interest were deliberately obscured by normal breast tissues. The "imaging" justification for "blending" is readily apparent; a cancer is visible in a mammogram because of its (slightly) higher X-ray attenuation which causes a lower radiation exposure on the film in the appropriate region of a projected image. Figure 12(b) shows an example of a mammogram whereby the mathematical phantom shown in Figure 12(a) has been blended into a clinically proven cancer free mammogram. The image shown was constructed by adding the amplitude of the mathematical phantom image to the cancer free mammogram followed by local smooth filtering of the combined image.

Figure 13(a) shows the result after processing the blended mammogram with unsharp masking. Figures 13(b) through 13(d) were obtained after reconstructing the blended mammogram from dyadic wavelet transform, φ-transform and hexagonal wavelet transform coefficients modified by multiscale edge sets identified automatically by our adaptive selection

Contrast values for local enhancement techniques					
Feature	$C_{Original}$	C_{UNS}	C_{DYA}	C_{PHI}	C_{HEX}
Minute microcalcification cluster	0.0504	0.0911	0.1488	0.1928	0.1391
Microcalcification cluster	0.0327	0.0479	0.1472	0.1022	0.1447
Spicular lesion	0.0241	0.0377	0.0849	0.0766	0.0848
Circular (arterial) calcification	0.0373	0.0601	0.1377	0.1250	0.1099
Well circumscribed mass	0.0115	0.0121	0.0225	0.0160	0.0263

Table 1: Contrast values for enhancement by unsharp masking (UNS) and local enhancement by multiscale edges obtained from dyadic wavelet (DYA), φ-transform (PHI) and hexagonal wavelet (HEX) coefficients.

Contrast Improvement Index (CII) for local enhancement techniques				
Feature	CII_{UNS}	CII_{DYA}	CII_{PHI}	CII_{HEX}
Minute microcalcification cluster	1.8051	2.9505	3.8226	2.7727
Microcalcification cluster	1.4628	4.4990	3.1225	4.4447
Spicular lesion	1.5651	3.5306	3.1860	3.5483
Circular (arterial) calcification	1.6126	3.6929	3.3533	2.9916
Well circumscribed mass	1.0510	1.9497	1.3857	2.3485

Table 2: CII for enhancement by unsharp masking (UNS) and local enhancement by multiscale edges obtained from dyadic wavelet (DYA), φ-transform (PHI) and hexagonal wavelet (HEX) coefficients.

technique described in Section 3.1.3. For purposes of comparing contrast, images within Figure 13 were rescaled by the same linear transformation.

Radiologists at Shands Hospital at the University of Florida have validated that processing the blended mammogram with such local enhancement techniques introduced no significant artifacts and preserved the shape of the known mammographic features (calcifications, dominant masses, and spicular lesions) contained in the original mathematical phantom. Figure 14 shows enlarged areas containing each feature in the processed mammogram for each method of contrast enhancement. As in Figure 13, images within each row of Figure 14 were rescaled by the same linear transformation. Enhancement by multiscale edges provided a significant improvement in local contrast for each feature included in the blended mammogram. A quantitative measure of contrast improvement can be defined by a Contrast Improvement Index (CII),

$$CII = \frac{C_{Processed}}{C_{Original}},$$

where $C_{Processed}$ and $C_{Original}$ are the contrasts for a region of interest in the processed and original images, respectively.

In this report we adopt a version of the optical definition of contrast introduced in [21]. The contrast C of an object is defined by

$$C = \frac{f - b}{f + b},$$

14

Contrast values for global enhancement techniques					
Feature	C_{HEQ}	C_{AHE}	C_{DYA}	C_{PHI}	C_{HEX}
Minute microcalcification cluster	0.0472	0.0302	0.1982	0.1993	0.2218
Microcalcification cluster	0.0296	0.1023	0.2040	0.2101	0.1919
Spicular lesion	0.0219	0.0437	0.1651	0.1641	0.1457
Circular (arterial) calcification	0.0390	0.1126	0.2136	0.2112	0.2013
Well circumscribed mass	0.0117	0.1586	0.1566	0.1499	0.1046

Table 3: Contrast values for enhancement by histogram equalization (HEQ), adaptive histogram equalization (AHE) and multiscale adaptive gain processing of dyadic wavelet (DYA), φ-transform (PHI) and hexagonal wavelet (HEX) coefficients.

Contrast Improvement Index (CII) for global enhancement techniques					
Feature	CII_{HEQ}	CII_{AHE}	CII_{DYA}	CII_{PHI}	CII_{HEX}
Minute microcalcification cluster	0.9352	0.5986	3.9290	3.9510	4.3968
Microcalcification cluster	0.9044	3.1258	6.2342	6.4210	5.8645
Spicular lesion	0.9092	1.8161	6.8613	6.8222	6.0558
Circular (arterial) calcification	1.0462	3.0201	5.7296	5.6633	5.3986
Well circumscribed mass	1.0165	13.7433	13.5757	12.9921	9.0705

Table 4: CII for enhancement by histogram equalization (HEQ), adaptive histogram equalization (AHE), and multiscale adaptive gain processing of dyadic wavelet (DYA), φ-transform (PHI) and hexagonal wavelet (HEX) coefficients.

where f is the mean gray-level value of a particular object in the image, called the *foreground*, and b is the mean gray-level value of a surrounding region called the *background*. This definition of contrast has the advantage of being independent of the actual range of gray levels in the image. With the aid of the mathematical phantom we computed local masks to separate the foreground and background regions of each feature included in the blended mammogram. Table 1 shows the contrast values for the mammographic features shown in Figure 14 while Table 2 shows the values for CII. Note that enhancement by multiscale edges performed significantly better than unsharp masking and consistently improved the contrast of each feature. Figures 15 through 17 show the improvement of local contrast accomplished by our local enhancement techniques for a sample scan line profile taken from cross sections of each feature. In all cases contrast was improved by local enhancement of edges while preserving the overall shape of each feature profile.

Figure 18(a) shows the result after processing the blended mammogram with adaptive histogram equalization (AHE). Figures 18(b) through 18(d) were obtained after reconstructing the blended mammogram from dyadic wavelet transform, φ-transform and hexagonal wavelet transform coefficients modified by multiscale adaptive gain processing. Figure 19 shows enlarged areas containing each feature in the processed mammogram for each method of contrast enhancement. For comparison of contrast, images within Figures 18 and 19 were rescaled

collectively as in Figures 13 and 14, respectively. Tables 3 and 4 show the contrast values and CII of the mammographic features displayed in Figure 19. Note that adaptive gain processing provided the maximum CII value for the minute microcalcification cluster, while histogram equalization and adaptive histogram equalization significantly decreased the contrast of this feature, possibly introducing diagnostic errors (false negatives). Although adaptive histogram equalization provided the maximum CII value for the well defined mass, it is clear from Figure 19 that multiscale adaptive gain processing better preserved the morphology of the mass and its surrounding structures.

(a)   (b)   (c)
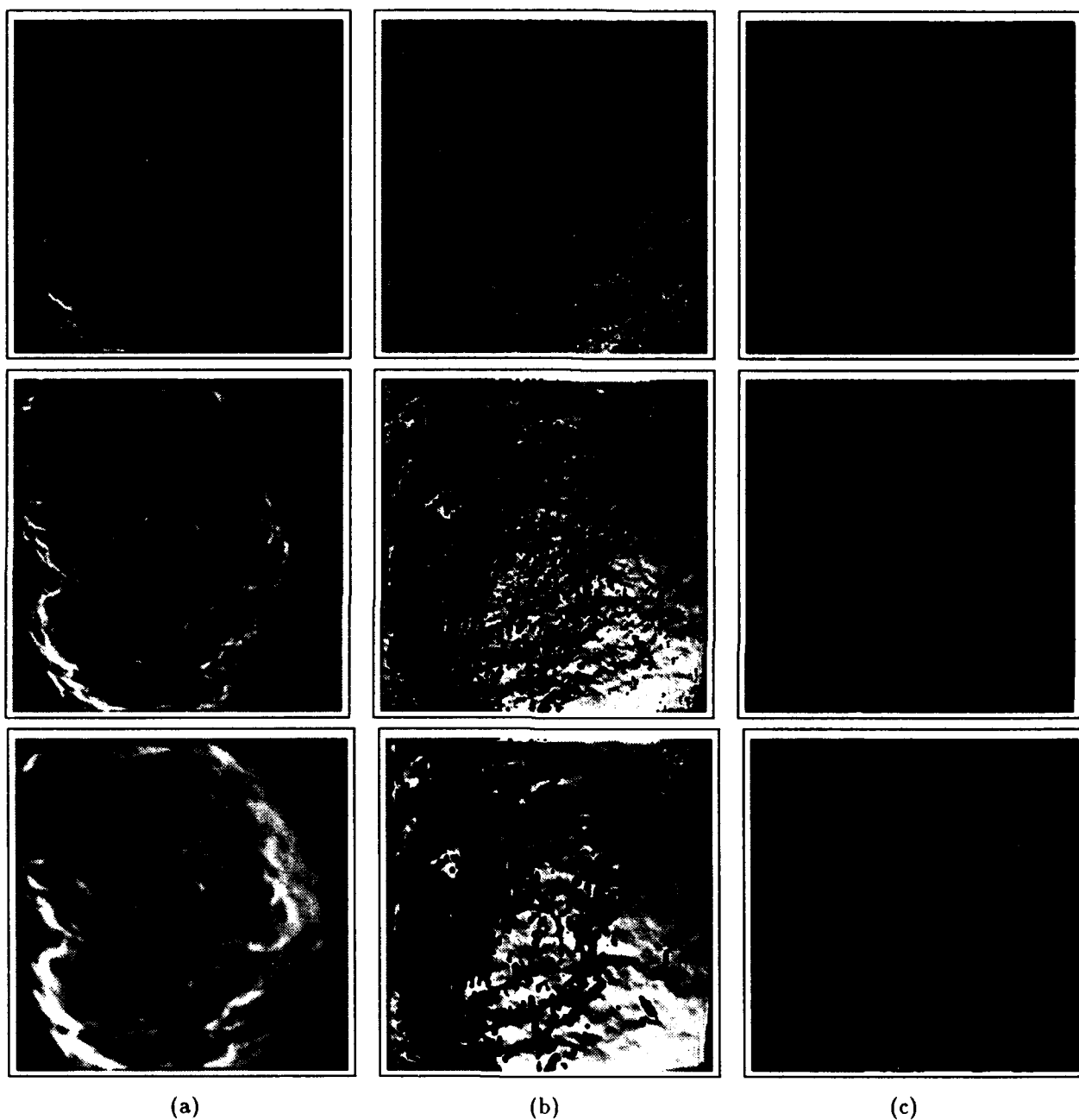
Figure 6: (a) Combination of horizontal and vertical components of dyadic wavelet coefficients for levels 1,2 and 3, respectively (top to bottom). (b) Phase of the combined coefficients. (c) Two-dimensional wavelet maxima coefficients shown as binary edges.

17
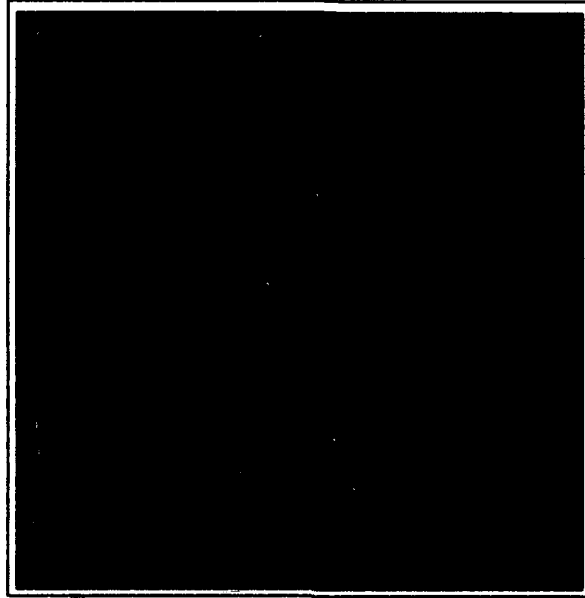
Figure 7: Combined orientations of φ edges obtained from level 4 coefficients.
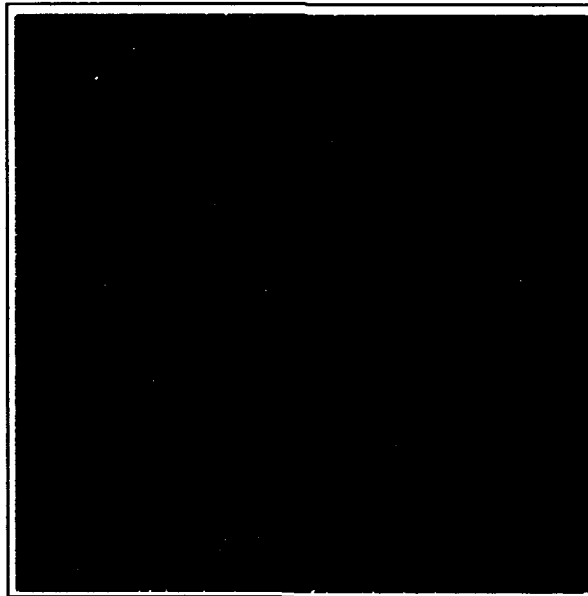
Figure 8: Combined orientations of hexagonal edges obtained from level 3 coefficients.
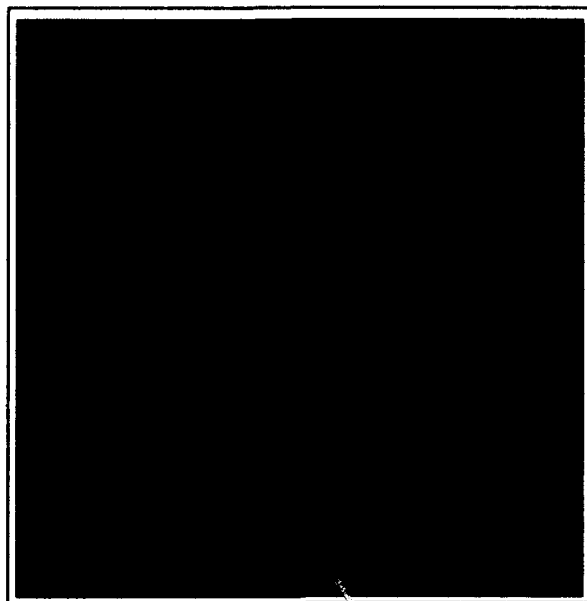
(a)
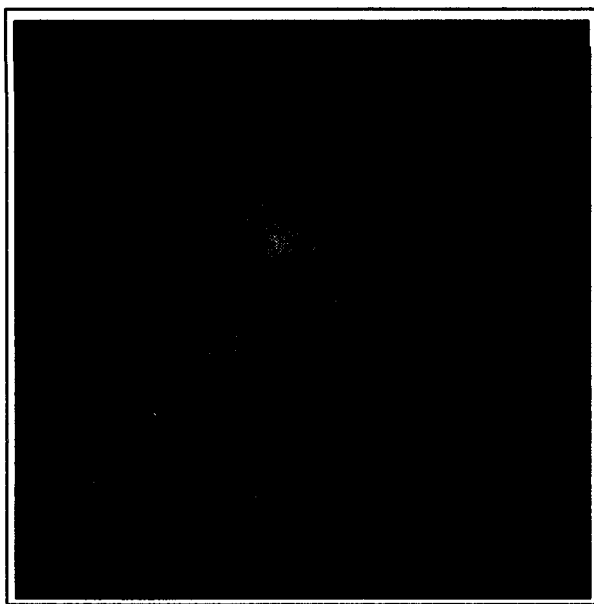
(b)
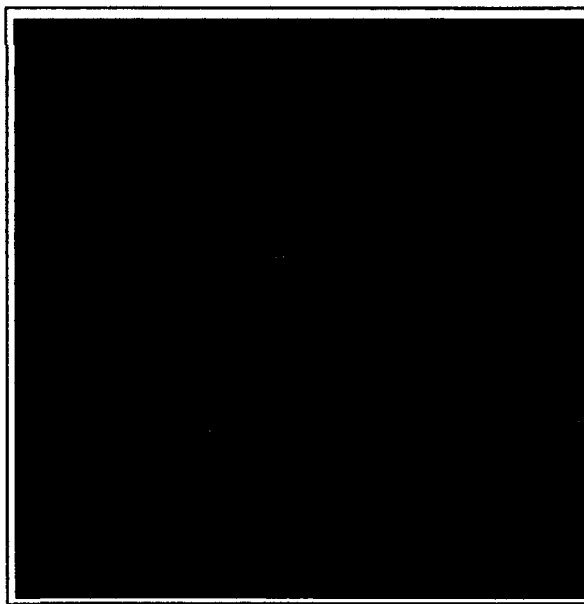
(c)

Figure 9: (a) Original dense mammogram, M41. (b) Enhancement by unsharp masking. (c) Local enhancement by the method of multiscale edges for dyadic wavelet transform coefficients.
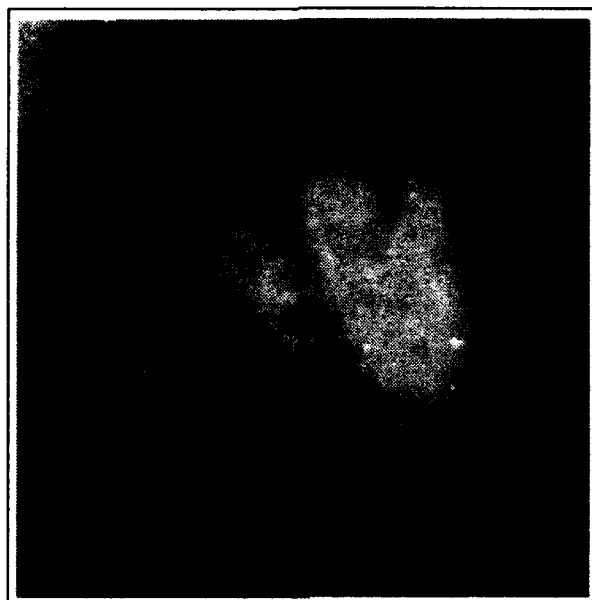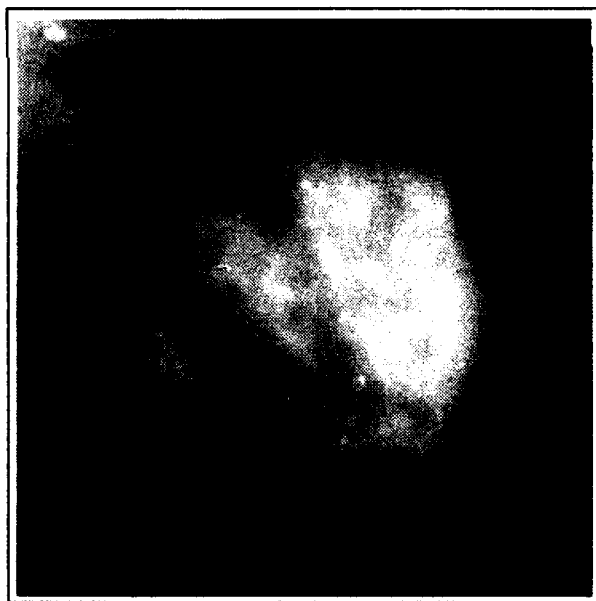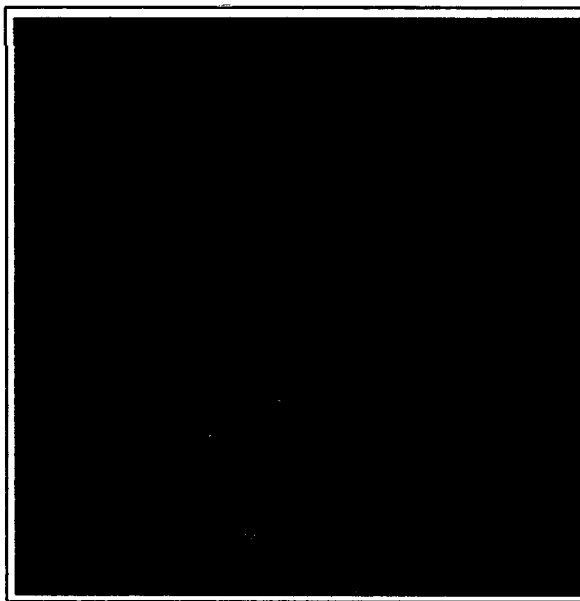
Figure 10: (a) Original dense mammogram, M56. (b) Enhancement by histogram equalization. (c) Global enhancement by multiscale histogram equalization of dyadic wavelet coefficients.
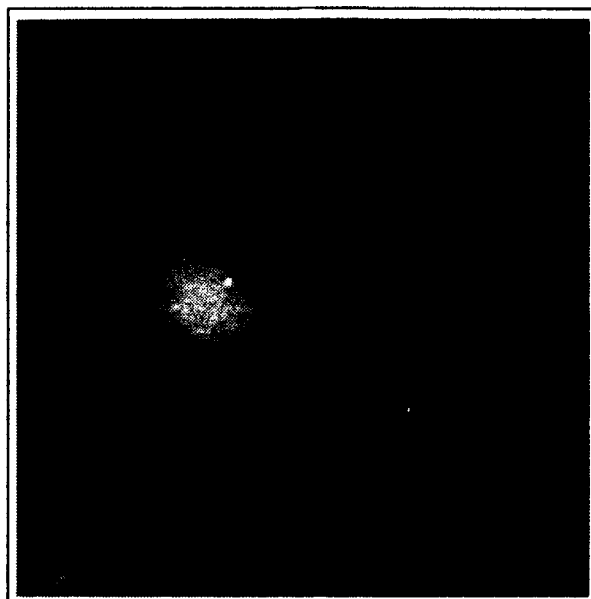
(a)

(b)
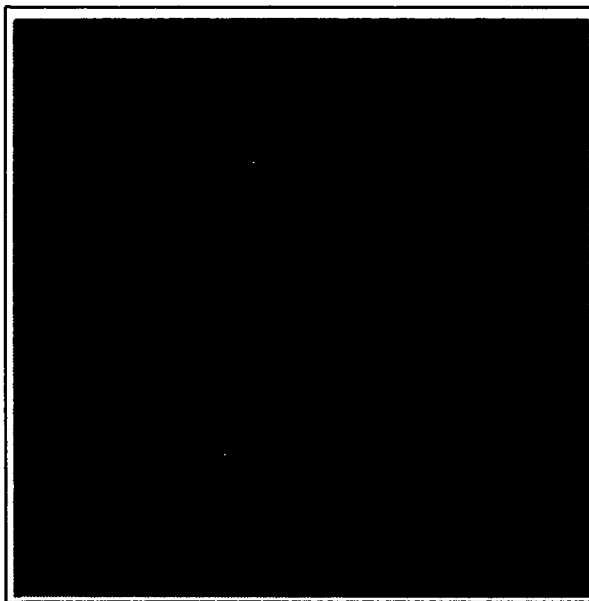
(c)

Figure 11: (a) Mammogram with spicular mass, M73. (b) Enhancement by adaptive histogram equalization. (c) Global enhancement by multiscale adaptive gain processing of φ-transform coefficients.
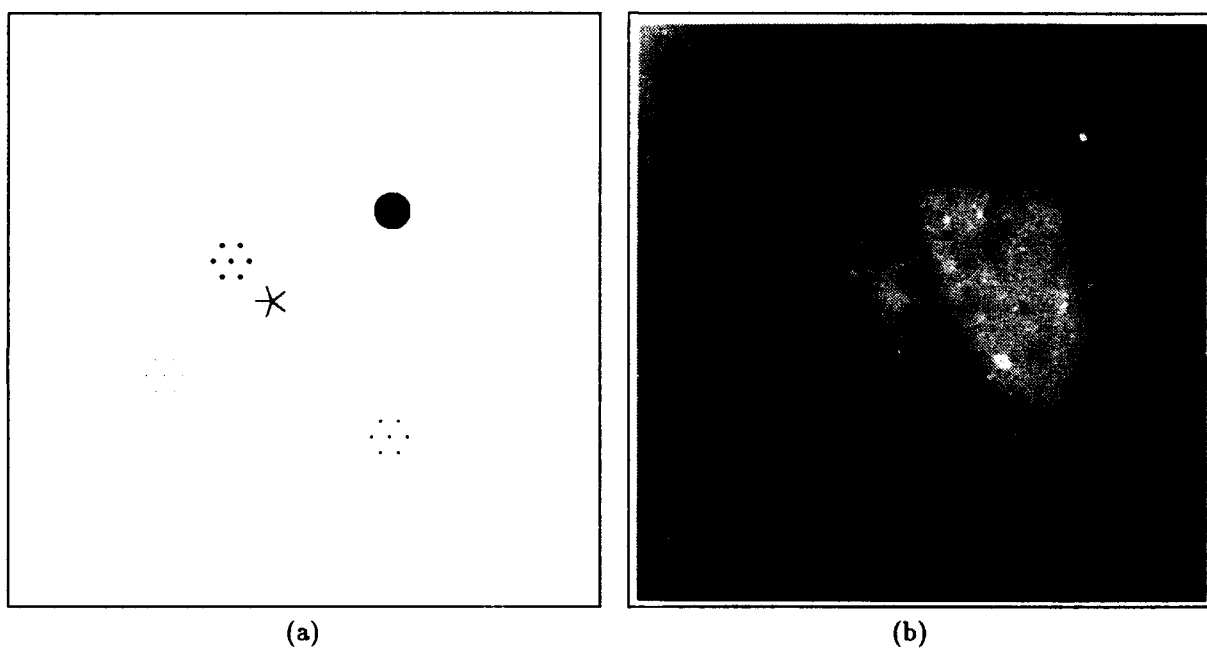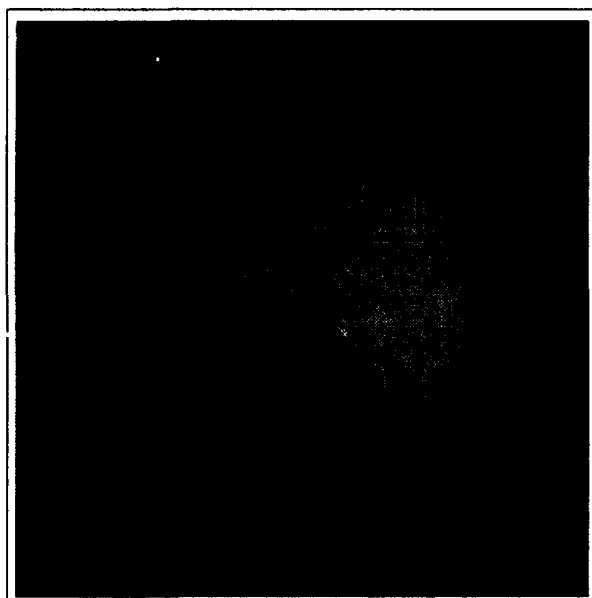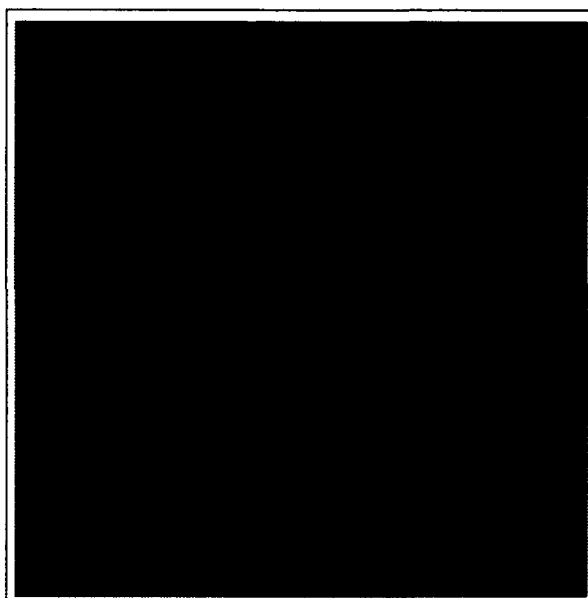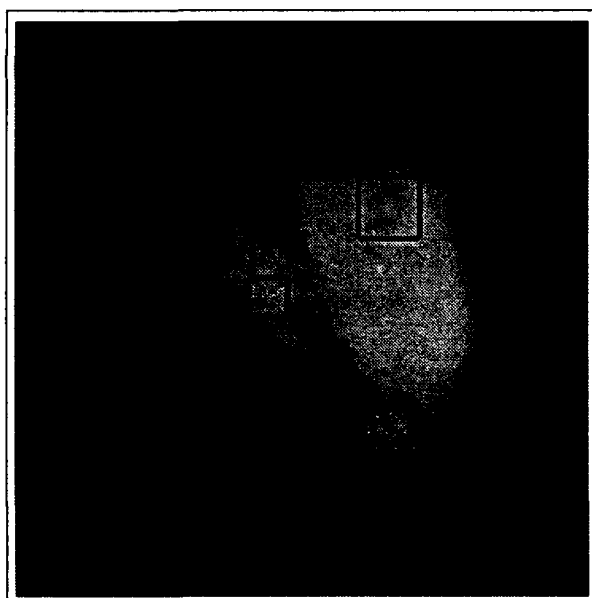
Figure 12: (a) Mathematical phantom. (b) Mammogram M56 blended with phantom shown in (a).
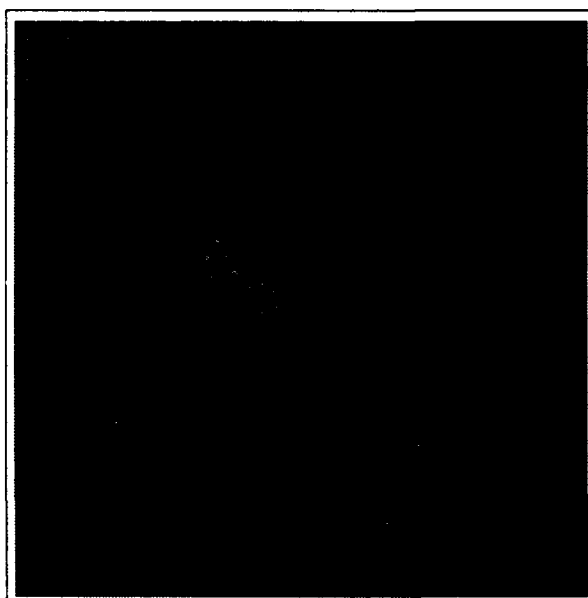
(a)

(b)

(c)

(d)

Figure 13: Blended mammogram: (a) Enhancement by unsharp masking. (b), (c) and (d) Local enhancement by multiscale edges obtained from dyadic wavelet transform. φ-transform and hexagonal wavelet transform coefficients. respectively.
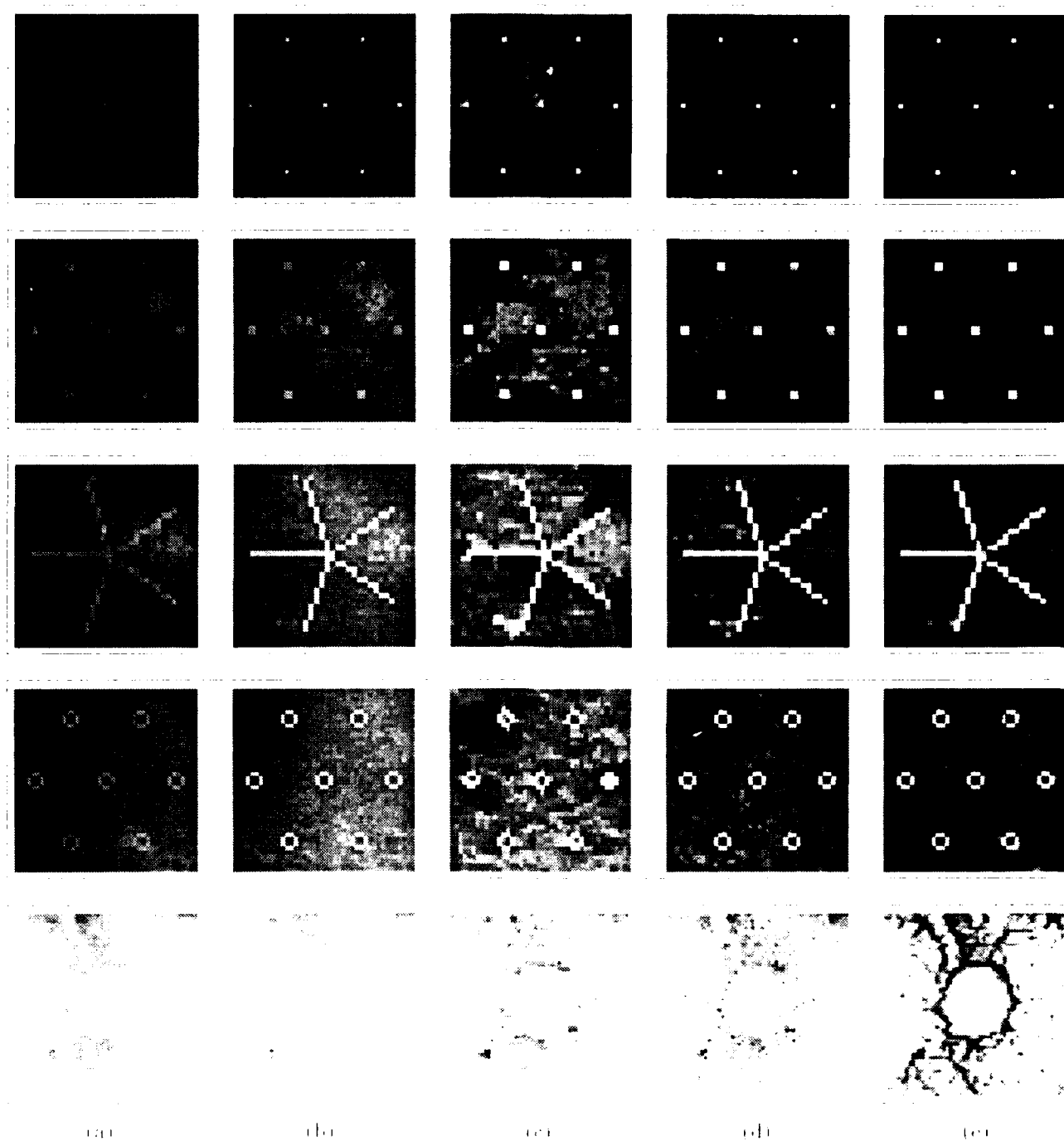
23

Figure 14: Contrast enhancement for features in blended mammogram. (a) Original image. (b) Enhancement by unsharp masking. (c), (d) and (e) Local enhancement by multiscale edges obtained from dyadic wavelet transform, φ transform and hexagonal wavelet transform coefficients, respectively. Phantom mammographic features from top to bottom: minute microcalcification cluster, microcalcification cluster, spicular lesion, circular (arterial) calcification and a well circumscribed mass.
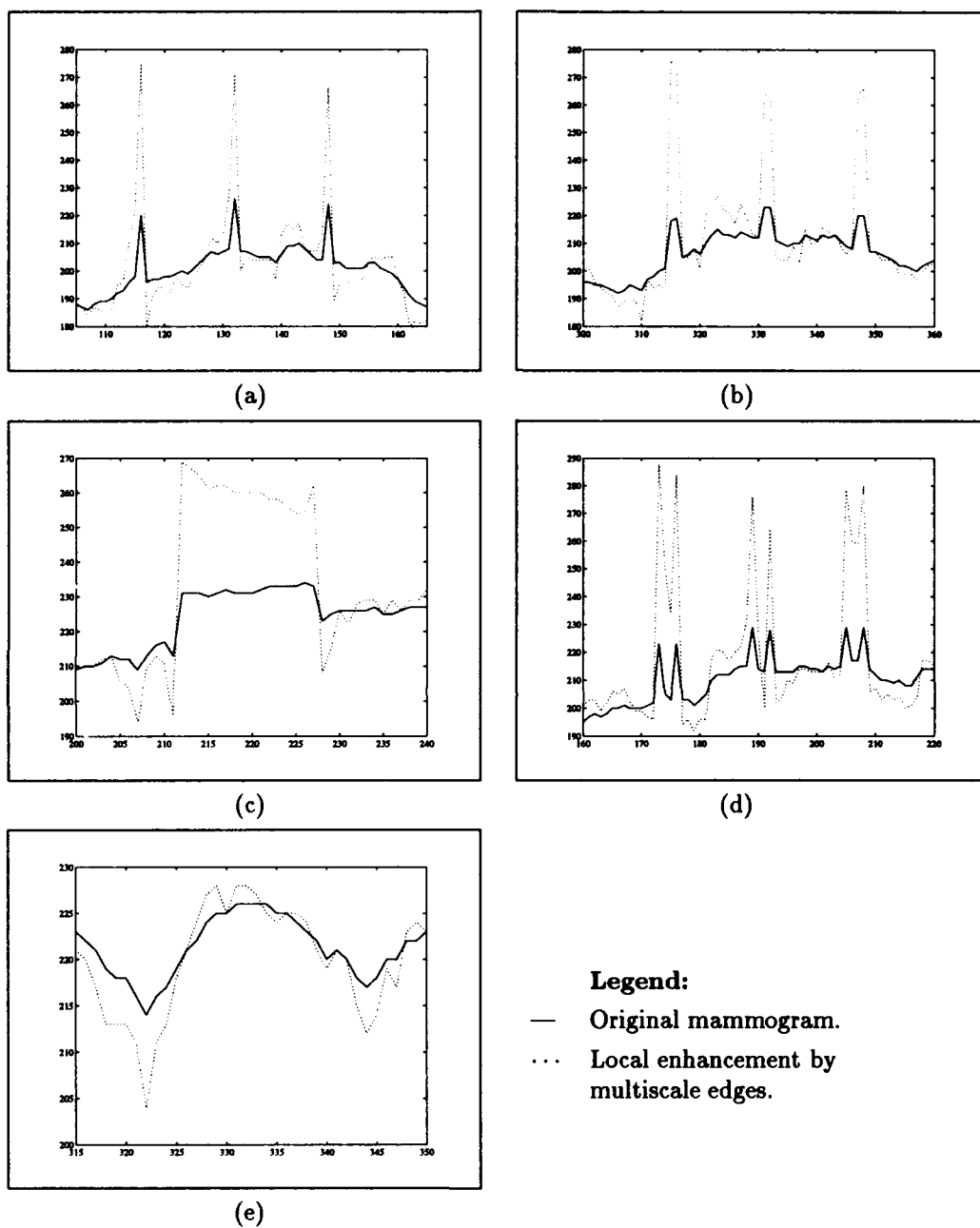
Figure 15: Sample scan lines displaying local enhancement by the method of multiscale edges for the dyadic wavelet transform: (a) minute microcalcification cluster, (b) microcalcification cluster, (c) spicular lesion, (d) circular (arterial) calcification and (e) well circumscribed mass.

(a)

(b)

(c)

(d)

(e)

Legend:

— Original mammogram.

··· Local enhancement by multiscale edges.

Figure 16: Sample scan lines displaying local enhancement by the method of multiscale edges for the φ-transform: (a) minute microcalcification cluster, (b) microcalcification cluster, (c) spicular lesion, (d) circular (arterial) calcification and (e) well circumscribed mass.

Figure 17: Sample scan lines displaying local enhancement for the method of multiscale edges for the hexagonal wavelet transform: (a) minute microcalcification cluster, (b) microcalcification cluster, (c) spicular lesion, (d) circular (arterial) calcification and (e) well circumscribed mass.
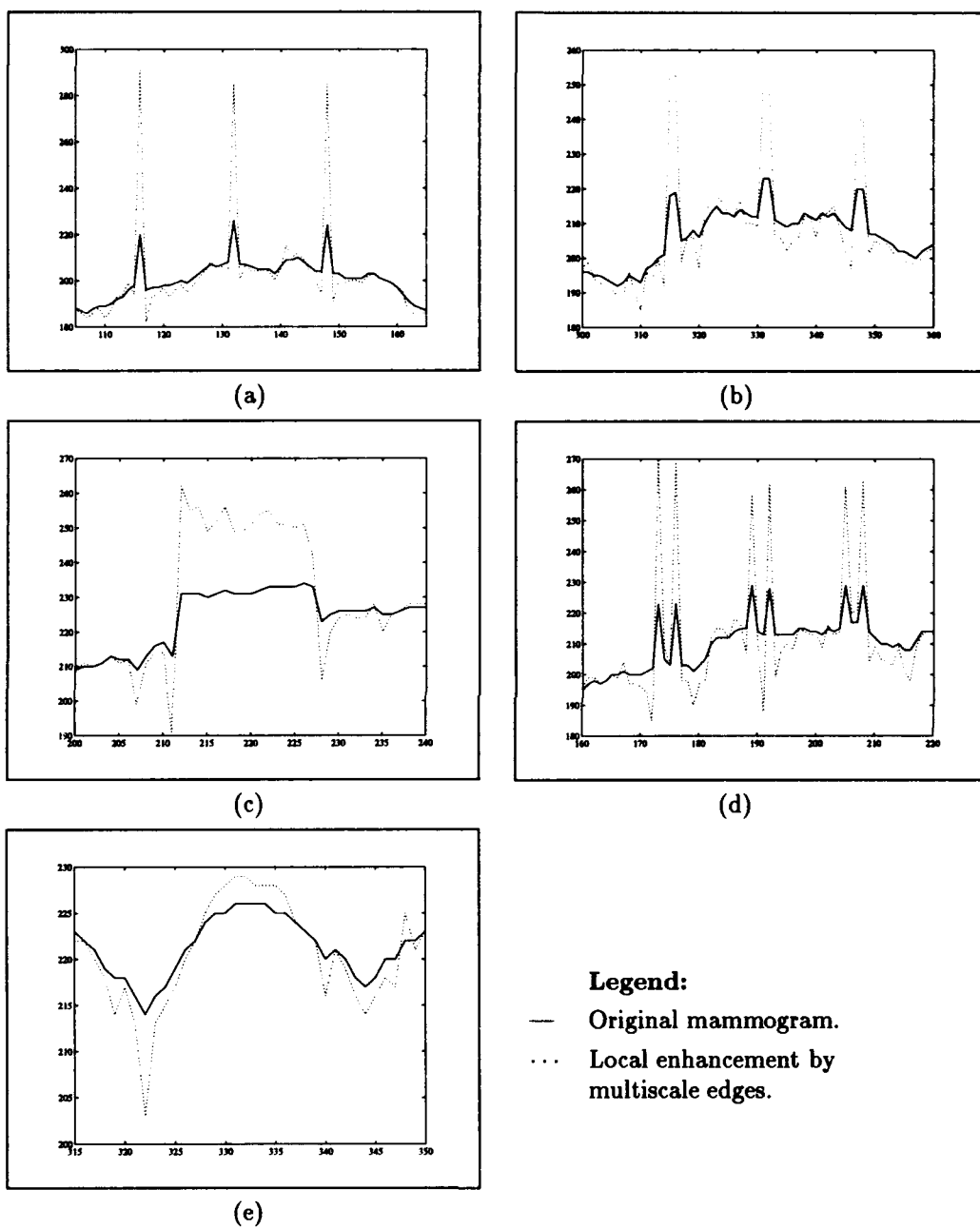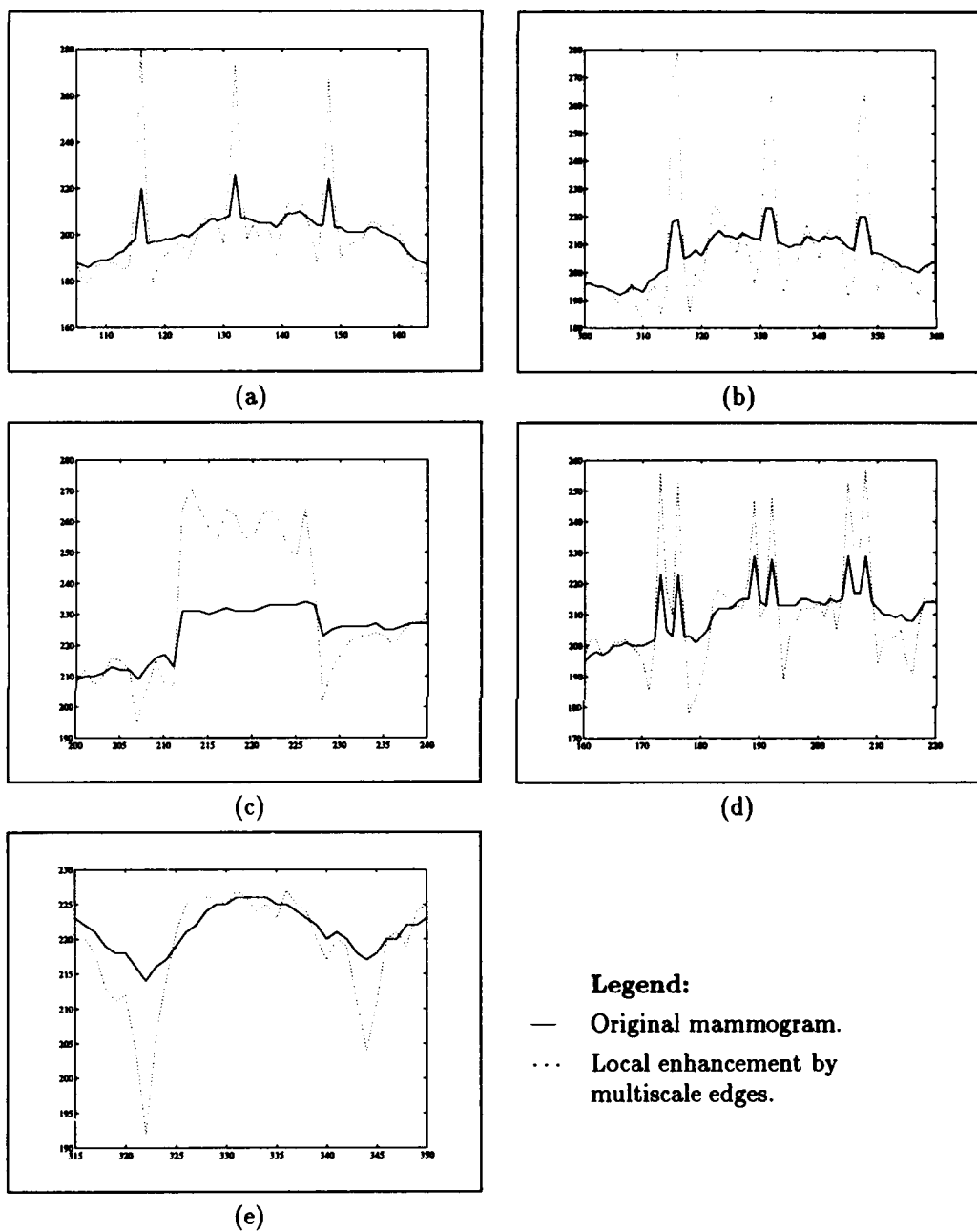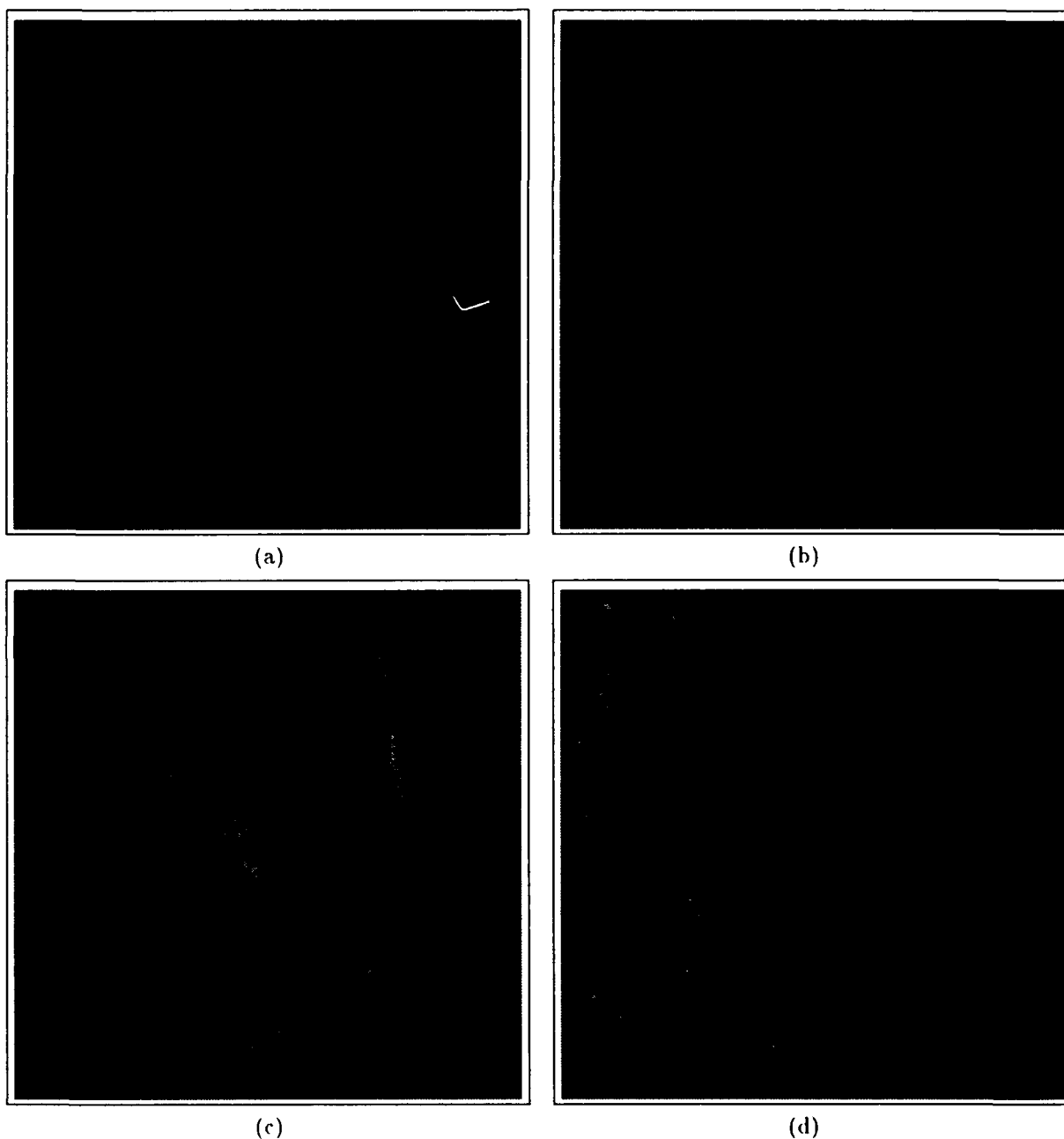
Figure 18: Blended mammogram: (a) Enhancement by adaptive histogram equalization. (b), (c) and (d) Global enhancement by multiscale adaptive gain processing of dyadic wavelet transform, φ-transform and hexagonal wavelet transform coefficients, respectively.

28

Figure 19: Contrast enhancement for features in blended mammograms. (a) Original image. (b) Enhancement by adaptive histogram equalization. (c), (d) and (e) Global enhancement by multiscale adaptive gain processing of dyadic wavelet transform, φ transform and 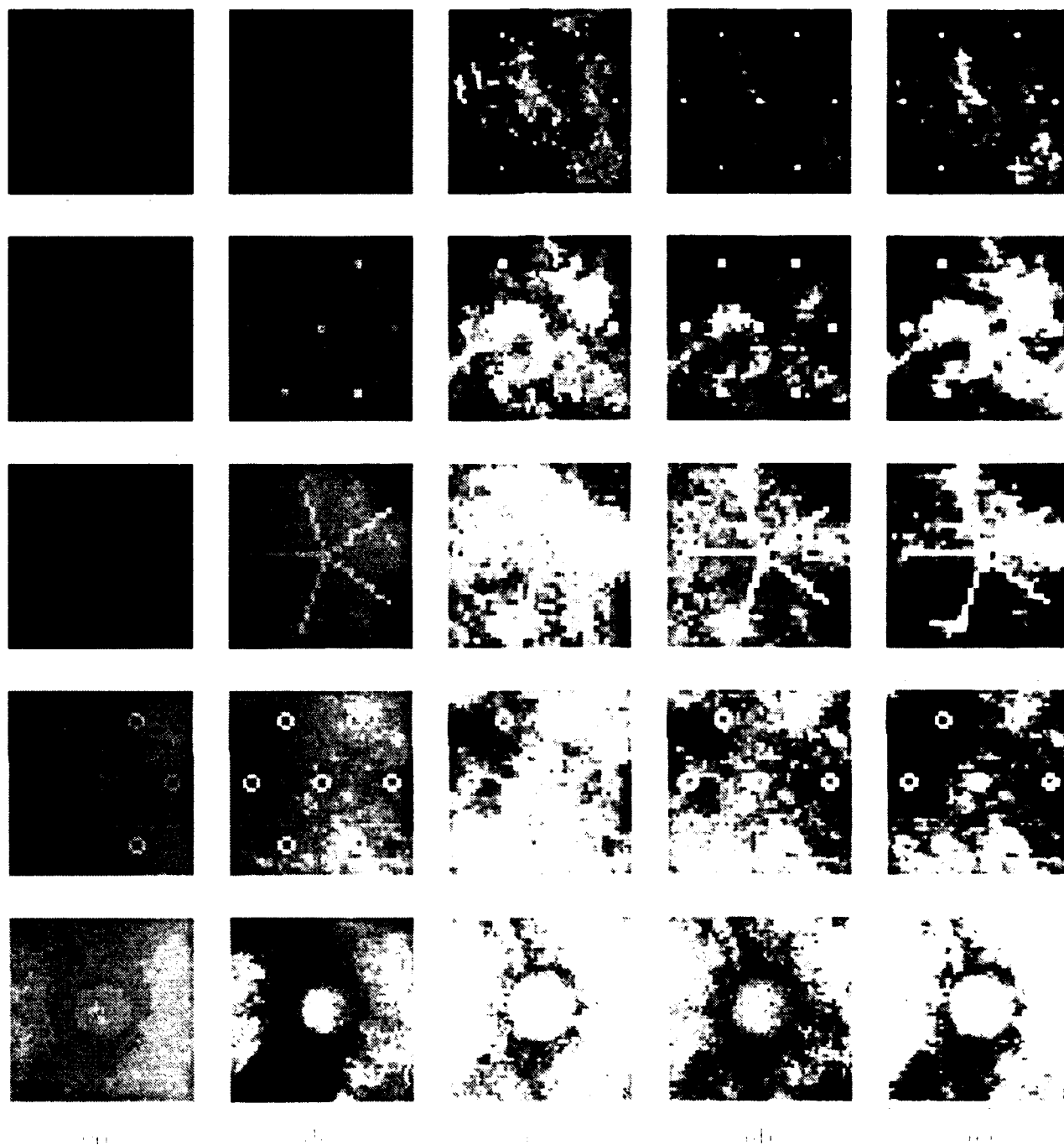hexagonal wavelet transform coefficients, respectively. Phantom mammographic features from top to bottom: minute microcalcification cluster, microcalcification cluster, spicular lesion, circular arterial calcification and a well-circumscribed mass.

2.4. Performance Evaluation

In this section we describe (1) the development of mathematical phantoms, (2) a measure of image quality, (3) evalutation techniques using radiographic phantoms, and (4) the design of a study to carry out clinical evaluations of processing mammograms.

2.4.1. Mathematical phantoms

The purpose of this task is to quantitatively and objectively evaluate the performance of wavelet processing algorithms (& any other type of image processing as well). Very good progress has been made in our attempt to develop appropriate measures of improvements achieved by image processing algorithms. The fundamental measure of image quality selected by our research group is the spatial frequency dependent parameter Signal to Noise Ratio [SNR(f)]. By obtaining the ratio of output SNRo(f) to input SNRi(f) values, the enhancement achieved can be measured.

A graduate student (Yisheng Zheng) has developed mathematical phantoms consisting of Gaussian signals and with random (Pojsson) noise added. Analysis of both signal and noise is achieved in the Fourier domain where the Gaussian signal is transformed using a Fast Fourier Transform (FFT). For the noise, the Auto-Correlation function is first computed and then its corresponding FFT obtained. The enhancement factor (EF) is given by $EF(f) = SNRo/SNRi$. This method is currently being applied systematically to investigate the properties of the dyadic wavelet, and the adaptive gain processing techniques described previously. A paper describing the method and results has been submitted for presentation at the *SPIE Mathematical Imaging: Applications of Wavelets to Signal and Image Processing*, in San Diego, July, 1994.

2.4.2. Image Quality Index

A recent publication by Desponds et al ("Image quality index (IQI) for screen/film mammography" Physics in Medicine and Biology 36 (1993) 19-33) proposed an intriguing metric for the measurement of image quality in mammography. A computer simulation of phantom images used by this Swiss mammographic research group to measure mammographic Image Quality directly is currently being developed by a graduate student (Yunong Xing). The computer simulated phantom will be used as an input to the wavelet processing algorithms described earlier to:

(a)   optimize wavelet processing parameters and

(b)   to evaluate any improvement in image quality achieved through image processing.

The initial application of this method shall be to the dyadic wavelet. A paper describing the method and initial results shall be submitted for presentation at the July 1994 SPIE meeting on Mathematical methods in Medical Imaging III in San Diego.

2.4.3. Radiographic phantoms

The Radiology department has recently acquired a LoRad biopsy system which has a digital imaging attachment capable of imaging a small region with a pixel size of 50 micons. During the next year, we plan to obtain images of physical phantoms, biopsy samples and clinical images which may then be digitally processed using the wavelet image processing algorithms. The usefulness of these methods of wavelet processing will be assessed by the measurement of imaging performance.

Another graduate student (Guoying Qu) has been developing psychophysical techniques to measure imaging performance using both objective and subjective techniques. Work has also begun on the development of suitable phantoms to be imaged to simulate features of interest to

mammography including microcalcifications, masses and spiculations. The work on evaluation of imaging performance is being prepared for presentation at the AAPM meeting in Los Angeles (August 1994) and for publication in the journal Investigative Radiology.

2.4.4. Clinical evaluations

A series of 20 mammograms with clinically proven malignant disease have been digitized and processed resulting in total of nine different mammograms. Processing techniques included dyadic, hexagonal and phi-wavelets; for each wavelet decomposition, three types of enhancement were performed including histogram equalization, edge enhancement and adaptive gain enhancement (as described in Sections 2.1 and 2.2 of this report). A graduate student (Carole Palmer) is currently working on the evaluation of these processed images. Key clinical questions that have been selected are as follows: Q1. Mass borders; Q2. Spiculations; Q3. Microcalcifications; Q4. Conspicuity of mass (relative to adjacent tissue); Q5. Internal architecture of mass; Q6. Architectural distortion of adjacent tissue by mass; Q7. Skin borders; Q8. Skin thickening. For each processed image the visibility of these features are compared with the original mammogram using the ranking scale: 1 = markedly less than original; 2 = less than original; 3 = similar to original; 4 = better than original; 5 = markedly better than original.

These results will provide a clear clinical guide to the areas where wavelet processing are most promising and the respective strengths and limitations of each type of wavelet and enhancement mode. As such, the work will complement the mathematical and radiographic evaluations described above. Initial results from this work are being presented at the 1993 RSNA meeting and will also be submitted for publication to Radiology.

2.5. Database for case studies

During the past year a Radiology Patient Information Data System (RAPIDS) for Mammography was developed for tracking patient clinical and pathology findings as well as for clinical management of patients. This will be used to identify candidates for wavelet processing evaluation.

The American College of Radiology (ACR) requires that data be kept on mammography patients so reminder letters can be sent, recommendations for treatment or additional studies can be followed up, status of outside film requests can be done, and mammography - pathology correlations can be calculated for each radiologist. Mammography software packages generally perform billing, results reporting, follow up reminders, and general practice management. At the University of Florida, billing and results reporting are done through the Radiology Information System, and the radiologists needed software to meet the ACR requirements and to keep track of data on needle localizations and implants. Prior to this project all data were kept manually on paper and using several non-integrated software packages.

Radiology Patient Information Data System (RAPIDS) was written for a PC using Clipper Database Management software that allows input of all relevant data and the generation of reports and letters. Paper data forms were designed to match the order in which data was entered on the computer for easy input. The data is organized in five main sections for input; patient demographics, image information, needle localization information, pathology diagnosis, and implant details. Complete patient histories are obtained and entered to calculate risk factors and to investigate risk factors in our patient population. Each study must have findings associated with it and all pathology findings are entered to calculate positive predictive values for each radiologist. A closing date for a record is entered when a patient dies or moves to another location to discontinue reminder letters for follow up examinations.

31

Although all data may be viewed for an individual patient, three categories of reports are also generated; patient information, radiologist reports, and summary reports on date ranges. Patient reports include: reminder letters based on the recommended time span between mammograms, list of requested outside films not yet received, patients based on age, family history of cancer, breast implants, and with other cancers. In addition, a list can be generated on patients with a particular radiological or pathologic finding. Radiologist reports include mammography - pathology correlation reports, recommendations for further studies and the results of those studies, and specific needle localization data. Summary reports include average case loads for each type of procedure, summary of cancer by stages as specified in the ACR report, summary of palpable and non-palpable cancers, and summary of cases based on findings.

Utilities included in the package perform daily and weekly backups with restore when necessary, allow additions to codes used in the database, and facilitate editing of data when necessary. In addition to all these features RAPIDS can easily be extended to a network environment and security features like password protection can be incorporated. A complete functional description of RAPIDS - a mammography database, shall be published in the procedings of SPIE Medical Imaging conference in February, 1994.

In addition to the database project, connections between the Dupont digitizer, Computer and Information Sciences(CIS), and an image archive were made. Software that converts Dupont native format images to ACR-NEMA was written and images were made available on the PACS network to CIS. Images sent back to Radiology in a raw raster file were converted to ACR-NEMA by creating an Interfile header (a European image standard developed for Nuclear Medicine) for each set of images then converting the image to ACR-NEMA for archival, display, and printing.

3. Conclusions

During the past year, we have developed a methodology for accomplishing adaptive contrast enhancement by multiscale representations. Our studies have demonstrated that features extracted from multiresolution representations can provide an adaptive mechanism for the local emphasis of salient and subtle features of importance to mammography. The improved contrast of mammographic features make these techniques appealing for computed aided diagnosis (CAD) and screening mammography. Screening mammography examinations are certain to grow substantially in the next few years, and analytic methods that can assist general radiologists in reading mammograms shall be of great importance. Thus, new applications for these representations should be targeted towards these two important areas.

The three analyzing functions investigated during the past year (dyadic wavelets, phi-transform, and hexagonal wavelets) were conceived as initial instances in the evolution of three *specialized detectors*. During the next year, we expect that these three "detectors" shall evolve through formulations that focus on three distinct types of mammographic features: (1) microcalcifications, (2) spicular lesions and (3) masses. The formulations driving these refinements shall be identified by the evaluation methods described in this report. In summary, we have exceeded the goals as described in our Statement of Work for the first year, and our research and development plans remain on schedule.

Below we list in summary, publications, presentations and talks accomplished by members of our research group during our first year.

Publications:

(1) Laine A, Schuler S, Fan J, Huda W, "Mammographic Feature Enhancement by Multiscale Analysis," to appear in *IEEE Transactions in Medical Imaging*.

(2) Laine A, Schuler S, Huda W, Honeyman JC and Steinbach BG, "Hexagonal wavelet processing of digital mammography," *SPIE Proceeding of Medical Imaging*, Volume 1898 (1993), pp. 559-573.

(3) Laine A, Song S, Laine A, Huda, W, Honeyman JC and Steinbach BG, "Adaptive multiscale processing for contrast enhancement," *SPIE Biomedical Image Processing and Biomedical Visualization*, Volume 1905 (1993), pp. 521-532.

Presentations (& published abstracts):

(1) Laine A, Huda W, Honeyman JC, Steinbach BG, "Mammographic image processing using wavelet processing techniques," Medical Physics 20 (1993) p. 1588 (Presented at the Fourth annual meeting of the Canadian Organization of Medical Physicists, Ottawa 12-15 May 1993).

(2) Laine A, Huda W, Honeyman JC, Steinbach BG, "Mammographic image processing using wavelet processing techniques," Medical Physics 20 (1993) p. 921 (Presented at the 35th Annual meeting of the American Association of Physicists in Medicine, Washington DC 8-12 August 1993).

(3) Laine W, Huda W, Honeyman JC and Steinbach BG, "Mammographic image processing using wavelet processing techniques," Scientific Program and Abstracts p. 96, 8th European Congress of Radiology, Vienna 12-17, September 1993.

(4) Steinbach BG, Laine A, Honeyman JC and Huda W, "Mammography image enhancement by using wavelet transforms," Radiology 189 (P) 1993 p. 105 (Presented at the 79th Annual meeting of the Radiological Society of North America, Chicago 28 November - 3 December 1993).

Invited Talks:

(1) Laine A, "Mammographic feature enhancement by multiscale analysis," Division of Mathematics and Image Processing, National Institutes of Health, Bethesda, MD, October 6, 1993.

(2) Laine A, "Wavelet processing techniques for digital mammography," and "Fundamentals of wavelet analysis," Department of Radiology, University of Chicago, October 4, 1993.

(3) Huda W, "Digital mammography and wavelets image processing," presented at the Bradford Royal Infirmary, Yorkshire, England 2 September 1993.

(4) Huda W, "Digital mammography and wavelets image processing," presented at the University of Manchester College of Medicine, England, 6 September 1993.

(5) Huda W, "Digital mammography and wavelets image processing," presented at Hammersmith Hospital, Royal Postgraduate Medical School, London, England, 10 September 1993.

References

[1] E.H. Adelson, E. Simoncelli, R. Higorani. Orthogonal pyramid transforms for image coding. In, *Proceedings of SPIE*, October 1987.

[2] I. Brodie, R.A. Gutcheck. Radiographic information theory and application to mammography, *Medical Physics*, Vol. 9, 79, 1982.

[3] A.C. Bovik, T.S. Huang, D.C. Munson. The effect of median filtering on edge estimation and detection. *IEEE Transactions on Pattern Analysis and Machine Intelligence.* Vol. PAMI-9: 181–194, 1987.

[4] I. Daubechies. Orthonormal bases of compactly supported wavelets.*Communications on Pure and Applied Mathematics.* Vol. 41: 909-996, 1988.

[5] I. Daubechies. The wavelet transform, time-frequency localization and signal analysis. *IEEE Transactions on Information Theory.* Vol. 36(5): 961–1005, 1990.

[6] L.S. Davis, A. Rosenfield. Noise cleaning by iterated local averaging. *IEEE Transactions on Systems, Man and Cybernetics.* Vol. SMC-8: 705–710, 1978.

[7] A.P. Dhawan, G. Buelloni, R. Gordon. Enhancement of mammographic feature by optimal adaptive neighborhood image processing. *IEEE Transactions on Medical Imaging.* Vol. MI-5:8, 1986.

[8] A.P. Dhawan, R. Gordon. Reply to comments on enhancement of mammographic feature by optimal adaptive neighborhood image processing. *IEEE Transactions on Medical Imaging.* Vol. MI-6:82, 1987.

[9] A.P. Dhawan, E. Le Royer. Mammographic feature enhancement by computerized image processing. *Computer Methods and Programs in Biomedicine,* Vol. 27: 23, 1988.

[10] R. Gordon, R.M. Rangayyan. Feature enhancement of film mammograms using fixed and adaptive neighborhoods. *Applied Optics.* Vol. 23:560, 1984.

[11] S.M. Lai, X. Li, W.F. Bischof. On techniques for detecting circumscribed masses in mammograms. *IEEE Transactions on Medical Imaging.* Vol. MI-8(4), 1989.

[12] A. Laine, W. Ball, A. Kumar. A multiscale approach for recognizing complex annotations in engineering documents. *IEEE Computer Society Conference on Computer Vision and Pattern Recognition,* Lahaina, Maui, Hawaii, June 3–6, 1991.

[13] A. Laine. Multiscale wavelet representations for mammographic feature analysis. In *Image Enhancement Techniques: Computer Science, National Cancer Institute Breast Imaging Workshop: State-of-the-Art and New Technologies,* Bethesda, MD, September 1991.

[14] A. Laine, S. Song. Multiscale wavelet representations for mammographic feature analysis. In *Proceedings of SPIE: Conference on Mathematical Methods in Medical Imaging,* San Diego, CA, July 23–25, 1992.

[15] A. Laine, S. Song. Wavelet processing techniques for digital mammography. In *Proceedings of SPIE: Conference on Visualization in Biomedical Computing,* Chapel Hill, NC, October 13–16, 1992.

[16] S. Mallat, S. Zhong. Complete signal representation with multiscale edges, New York University, Computer Science Technical Report 483, December 1989.

[17] S. Mallat. A Theory for Multiresolution Signal Decomposition: The Wavelet Representation. *IEEE Transactions on Pattern Analysis and Machine Intelligence.* Vol. 11(7): 674–693, 1989.

[18] S. Mallat. Multiresolution approximations and wavelet orthonormal bases of $L^2(R)$. *Transactions of the American Mathematical Society.* Vol. 315(1): 69–87, 1989.

[19] S. Mallat. Time-frequency channel decompositions of image and wavelet models. *IEEE Transactions on Acoustics, Speech, and Signal Processing.* Vol. ASSP-31, No. 1, 1989.

[20] S. Mallat, S. Zhong. Signal characterization from multiscale edges. In *10th International Conference on Pattern Recognition,* 891–896, 1990.

[21] W.M. Morrow, R.B. Paranjape, R.M. Rangayyan, J.E.L. Desautels. Regio-based contrast enhancement of mammograms. *IEEE Transactions on Medical Imaging.* Vol. 11(3): 392–406, 1992.

[22] M. Nagao, T. Matsuyama. Edge preserving smoothing. *Computer Graphics and Image Processing.* Vol. 9: 394–407, 1979.

[23] A. Scheer, F.R.D. Velasco, A. Rosenfiled. Some new image smoothing techniques. *IEEE Transactions on Systems, Man and Cybernetics.* Vol. SMC-10(3): 153–158, 1980.

[24] E.P. Simoncelli, E.H. Adelson. Non-separable Extensions of Quadrature Mirror Filters to Multiple Dimensions. *Proceedings of the IEEE,* Vol. 78, No. 4, April 1990.

[25] P.G. Tahoces, J. Correa, M. Souto, C. Gonzalez, L. Gomez, J. Vidal. Enhancement of chest and breast radiographs by automatic spatial filtering. *IEEE Transaction on Medical Imaging.* Vol. MI-10(3): 330-335, 1991.

[26] T.N. Wiesel, Postnatal development of visual cortex and the influence of environment (Nobel Lecture), Nature, Vol. 299, 583–591, 1982.